International Journal of Heavy Vehicle Systems

ISSN online: 1741-5152 - ISSN print: 1744-232X
https://www.inderscience.com/ijhvs

A FOPID based decentralised control system for vibration control of railway vehicle using hybrid optimisation

Nitish, Amit Kumar Singh

DOI: 10.1504/IJHVS.2023.10059063

Article History:

Received:	10 January 2023
Last revised:	02 May 2023
Accepted:	08 May 2023
Published online:	24 January 2024

A FOPID based decentralised control system for vibration control of railway vehicle using hybrid optimisation

Nitish and Amit Kumar Singh*

Department of Instrumentation and Control Engineering,
Dr. B. R. Ambedkar National Institute of Technology,
Jalandhar, Punjab, 144008, India
Email: nitish.ic.18@nitj.ac.in
Email: singhak@nitj.ac.in
*Corresponding author

Abstract: This paper proposes a 17-degree-of-freedom dynamic railway vehicle model integrated with wheel-rail forces and active suspensions. The passive response of the model is validated with the experimental results. Afterward, a decentralised control structure having fractional order proportional integral derivative (FOPID) controller has been formulated to mitigate the track disturbances. A novel metaheuristic optimisation technique named hybrid PSO-GWO has been proposed to provide the optimum force. The performance of FOPID controllers was evaluated in the time and frequency domain under the periodic and random track disturbances, and the results were compared against the passive system and classical tuning method. From the results, it is seen that hybrid PSO-GWO is more capable of reducing the vehicle accelerations as compared to other tuning methods as it can be able to reduce the lateral, roll, and yaw acceleration up to 77.81%, 75.29% and 63.74% under periodic and, 57.22%, 77.88%, and 69.58%, under random excitations.

Keywords: active suspension; decentralised control; FOPID controller; metaheuristic algorithms; power spectral density; ride comfort.

Reference to this paper should be made as follows: Nitish and Singh, A.K. (2024) ‘A FOPID based decentralised control system for vibration control of railway vehicle using hybrid optimisation’, *Int. J. Heavy Vehicle Systems*, Vol. 31, No. 1, pp.113–146.

Biographical notes: Nitish is a research scholar at the Dr. B. R. Ambedkar National Institute of Technology, Jalandhar, Punjab, India. He received his Bachelor and Master degree from Sant Longowal Institute of Engineering and Technology, Sangrur, Punjab, India in 2015, and 2018 respectively. His area of research includes the control theory, signal processing and optimisation.

Amit Kumar Singh is an Assistant Professor of Department of Instrumentation and Control Engineering at Dr. B.R. Ambedkar National Institute of Technology, Jalandhar, Punjab, India. He has done his Doctorate and Masters from IIT Roorkee and NIT Kurukshetra, respectively. His area of expertise are control systems, optimisation and applications of soft computing in renewable energy.

1 Introduction

In recent years, commercial demand for comfortable and quiet vehicles has encouraged the industrial development to accommodate a balance of performance, efficiency, and comfort levels. Particularly, the noise, vibration, and harshness characteristics of railway vehicles, trucks, cars, and tractors are becoming increasingly important (Oesterling et al., 1999; Peng and Lines, 1997; Ranganathan and Mohan, 1997). Among them, the importance of railways to international trade and global development is self-evident. Over the past few decades, the railway industries have concentrated on increasing train speed while enhancing travel comfort and safety. However, faster trains and the presence of track abnormalities will significantly raise the vibration level, lowering the stability and pleasure of the trip. In order to improve ride comfort and safety, vehicle vibrations must be reduced. Two approaches can be used to address these vibration issues:

1 improving the state of the railway rails

2 improving the vibration mitigation system.

Since the track cannot be altered once built, the second strategy of improving vibration mitigation systems is more practicable.

According to prior research, three types of vibration mitigation systems are considered in car suspensions: passive, semi-active, and active (Karkoub and Zribi, 2006). A passive system comprises low-cost static springs and oil/pneumatic dampers. Despite the low cost and simple design, the passive system does not deliver acceptable control performances in terms of ride comfort or quality (Miller , 1988). A semi-active system, on the other hand, is outfitted with a variable gain damper filled with a rheological fluid whose viscosity changes when exposed to an electric or magnetic field. Electro-rheological (ER) and magneto-rheological (MR) rheological fluids are utilised in semi-active suspension and are responsible for variable damping (Rabinow, 1948; Winslow, 1947). Several previous research papers have discussed the use of ER and MR fluid in semi-active suspension to minimise vibrations (Choi et al., 1998; Sims and Stanway, 2003; Wang and Liao, 2009a; Wei et al., 2016; Wu and Griffin, 1997; Zong et al., 2013). The MR-based damper is the most successful because it generates more power and has a wider operating temperature range than an ER damper. However, the complex control techniques of a semi-active suspension system make it difficult to successfully suppress vibrations across the excitation's wide frequency range (Wang et el., 2009). Thus, researchers discovered an alternate vibration control method in the form of active suspension by realising the limitations of both passive and semi-active systems (ElMadany and Samaha, 1992). An active suspension system (ASS) combines the passive components with controller-controlled actuators that generate extra force (Wang, 2020). It can continually reduce the vehicle's vibrations over a wide range of frequencies and provide better ride comfort (Fu et al., 2020; Hrovat, 1990; Yoshimura et al., 1993).

Using various control structures and algorithms, the system controller calculates the amount of extra force required to suppress the vibrations. In the past, several research papers on traditional and innovative controllers to maximise the performance of ASSs have been published. These include the use of proportional integral derivative (PID) control (Afolabi Daniyan and Mpofu, 2019; Daniyan et al., 2019, 2018; Metin and Guclu, 2014, 2011), fuzzy logic control (Kalaivani et al., 2014; Sezer and Atalay, 2011), sliding mode control (Choi et al., 2000; He et al., 2020), neuro-fuzzy control (Nguyen and Nguyen, 2017), model predictive control (Orukpe, 2013; Orukpe et al., 2008), optimal control (Olivier et al., 2021; Graa et al., 2018; Molatefi et al., 2017; Hrovat, 1993; Reina et al., 2016) and neural-network-based control (Atray and Roschke, 2004; Eski and Yildirim, 2009; Li et al., 2021). Because of its simple and durable performance under various operating situations, the proportional integral derivative (PID) controller is a favourite in modern control domains. The PID controller's performance is determined by the values of three parameters K_P, K_i, and K_d, which need to be optimally tuned according to the desired output. The traditional tuning methods such as Ziegler-Nichols (ZN) and Cohen-Coon (CC), which were previously thought to be the best, are now being supplemented by heuristic optimisation techniques because traditional methods may fail to provide the desired performance in terms of overshoot, settling time, and steady state error. Furthermore, if the order of the system increases, the performance of the PID controller may degrade. Because the real-world applications are well represented in terms of higher fractional order, these limitations of PID controller can be overcome by using fractional order PID (FOPID) combining with heuristic or meta-heuristic optimisation algorithms (Stephen Bassi Joseph et al., 2022).

Oustaloup et al. first put up the idea of FOPID controllers in 1991. It is a more sophisticated form of traditional PID since it has five tuning parameters (K_P, K_i, K_d, λ and μ) instead of three, which allows for more design flexibility. Duarte Valerio et al. (Valério and da Costa, 2006) proposed two sets of tuning for FOPID using the same method as that of Z-N, and the results were successfully observed on first-order plus time delay processes. A comparative study of tuning FOPID in the time and frequency domain has been given by Das et al. (2011). The results demonstrate the superiority of the frequency domain technique over the time domain in terms of noise rejection and robustness. Cao et al. (2005) presented a GA-based FOPID controller for providing good dynamic response and stability in various systems. The successful implementation of FOPID using PSO, ACO, and GA for automatic voltage regulator systems (AVRS) has been reported in Babu et al. (2016) and Kim and Park (2005), respectively. Gad et al. (2015, 2017) employed GA to optimise the parameters of FOPID and PID used for semi-active suspensions, in which semi-active suspension with a human body model was used to investigate the influence of vertical vibration. Verma et al. (2017) use GWO optimisation to tune the parameters of FOPID, and the simulation has been performed for higher order and time-delay process. The effect of adding fractions to control the DC servo motor velocity has been analysed by Barbosa et al. (2010), in which the ZN tuning method was used to tune the parameters of the fractional order controller. The implementation of PSO-based FOPID for a second-order system has been successfully reported by Dastranj et al. (2012). A comparison of PSO and ABC-based FOPID has been performed for second order system with time delay (Bingul and Karahan, 2018), and the robustness of the controller has been checked by using different cost functions such as mean square error (MSE), mean time square error (MTSE). Alamdar Ravari and Yaghoobi (2019) proposed a chaotic firefly algorithm to tune the parameters of FOPID for a continuous stirred tank reactor (CSTR). The output shows better results than integer order PID in terms of overshoot, settling time, and steady-state error. Shivam Jain et al. (Jain and Hote, 2020) proposed a new technique for tuning FOPID using modified

ZN rules and a big bang crunch optimisation algorithm, and results are verified on different applications.

According to the literature, FOPID controllers with meta-heuristic optimisation have been employed for various applications, including chemical processes, motor speed control, sun tracking systems, vibration control, voltage regulation systems, and many more. However, just a few studies on FOPID have been published in the context of vibration control employing an ASS. Moreover, for a multi-input multi-output (MIMO) system, two types of control structures, i.e., centralised and decentralised, are reported in the literature (Luo et al., 2011). Whereas the majority of the research has been carried out using a centralised control structure, i.e., all data collected from an individual sensor is fed back to the central controller, this creates the problem of a large amount of data transmission at one time, as well as making the system complex. A decentralised or multi-loop control technique with a basic structure can solve the problem of massive data transfer (Lei and Wu, 2011; Lengare et al., 2012). As per the contribution of this study, a decentralised FOPID controller coupled with metaheuristic optimisation techniques for active suspension is provided, which is projected to deliver the best results that meet the need for enhanced ride comfort in railway cars. First, a 17-DOF dynamic model of a full-scale railway vehicle is created, complete with wheel-rail forces and active suspension. The governing equations of motion represent the translational and rotational motions of the car body, bogies, and wheelsets. Then, to suppress the vibration of the car body's lateral, roll, and yaw motion, a decentralised control system with three independent FOPID controllers is used. Two forms of periodic and random track irregularities, named lateral alignment and cross-level, are used as input to the vehicle to evaluate the control system's performance. To compute the optimal active force for the suspension system, a novel hybrid optimisation technique, hybrid PSO-GWO, was used. To validate the proposed work's performance, the FOPID is optimised using the ZN, PSO, and GWO, and the results are critically studied in the time and frequency domains. A comparison of the proposed metaheuristic algorithm and the passive system is also performed using root mean square (RMS) acceleration data. The analysis and simulation results based on the quadratic cost function reveal that the suggested controller performs well with optimal gains.

This paper is organised as follows: Section 2 focuses on the analytical model and experimental validation of railway vehicles with the track irregularities model discussed in Sections 3 and 4, respectively. The control scheme and structure adopted for vibration suppression are presented in Section 5, followed by Section 6, explaining the controller and optimisation approaches. The system responses based on the decentralised control structure are presented in Section 7. Then, the results and discussions are described in Section 8, and the conclusions are presented in Section 9.

2 Analytical model of the railway system

This section presents the dynamic model of railway vehicles, and state space models.

2.1 A 17-DOF dynamic model of a railway vehicle

The definitions of various symbols related to the vehicle body, bogies, and wheelset motion used in dynamic modelling are given in Table 1. In contrast, pictorial representations are given in Figure 1(a)–(c). The governing equations of motion of railway vehicle dynamics are presented as follows:

Table 1 Various symbols used in the modelling

Symbols	*Definitions*
Y_c, Y_{ti}, Y_{wj}	Lateral displacement of the car body, bogies, and wheelsets (i =1,2 & j =1,2,3,4)
θ_c, θ_{ti}	Roll displacement of the car body, bogie (i =1,2)
ϕ_c, ϕ_{ti}	Pitch displacement of the car body and bogie (i =1,2)
$\Psi_c, \Psi_{ti}, \Psi_{wj}$	Yaw displacement of the car body, bogie, and wheelsets (i =1,2 & j =1,2,3,4)
Y_{rj}, θ_{clj}	Rail track disturbances (j =1,2,3,4)

Figure 1 17-DOF analytical model of a railway vehicle: (a) end view; (b) front view and (c) top view

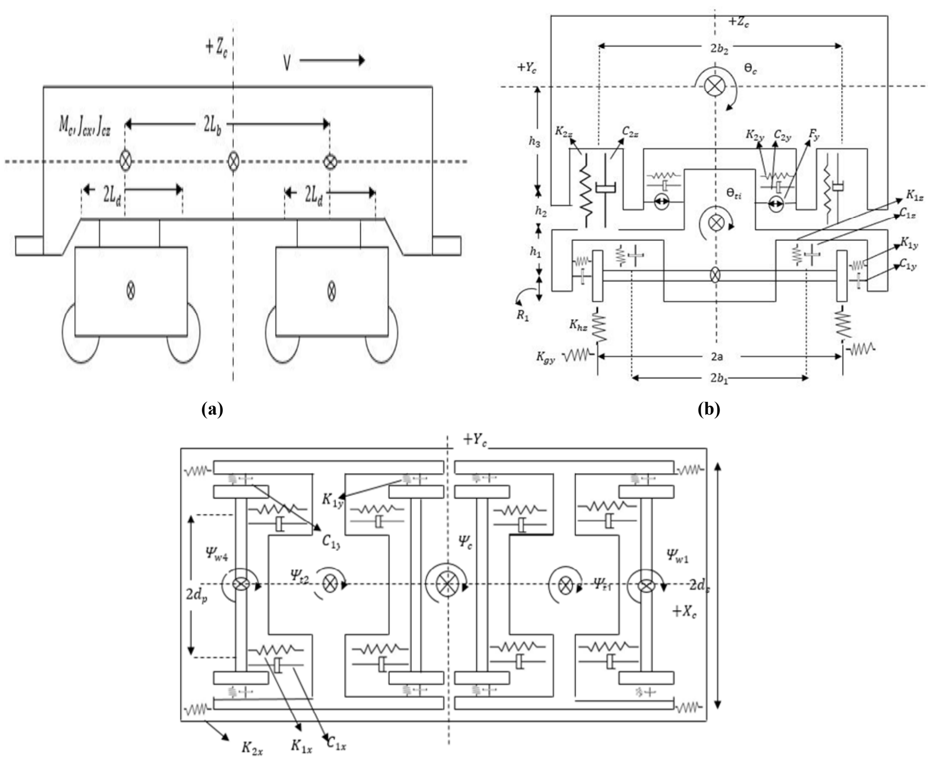

2.1.1 Vehicle body dynamics

$$M_c \ddot{Y}_c + 2K_{2y}\left[2\left(y_c + h_3\theta_c\right) - y_{t1} - y_{t2} - h_2\theta_{t1} - h_2\theta_{t2}\right] + 2$$
$$C_{2y}[2\left(\dot{y}_c + h_3\dot{\theta}_c\right) - \dot{y}_{t1} - \dot{y}_{t2} - h_2\dot{\theta}_{t1} - h_2\dot{\theta}_{t2}\Big] = [F_{y1} + F_{y2}] \tag{1}$$

$$I_{Xc}\ddot{\theta}_c + 2b_2^2K_{2z}\left(2\theta_c - \theta_{t1} - \theta_{t2}\right) + 2b_2^2c_{2z}\left(2\dot{\theta}_c - \dot{\theta}_{t1} - \dot{\theta}_{t2}\right) + 2h_3K_{2y}\{2\,($$
$$y_c + h_3\theta_3) - y_{t1} - y_{t2} + h_2\theta_{t1} + h_2\theta_{t2}) + 2h_3c_{2y}(2\left(\dot{y}_c + h_3\dot{\theta}_3\right) - \dot{y}_{t1} - \dot{y}_{t2} + h_2\dot{\theta}_{t1} \mp \dot{\theta}_{t2}\Big] =$$
$$[h_3\left(F_{y1} + F_{y2}\right) + b_2(\left(F_{z1} + F_{z3}\right) - \left(F_{z2} + F_{z4}\right)) \tag{2}$$

$$I_{Zc}\ddot{\Psi}_c + 2L_bK_{2y}\left(2L_b\Psi_c - y_{t1} + y_{t2} - h_2\theta_{t1} + h_2\theta_{t2}\right)$$
$$+2L_bC_{2z}\left(2L_b\dot{\Psi}_c - \dot{y}_{t1} + \dot{y}_{t2} - h_2\dot{\theta}_{t1} + h_2\dot{\theta}_{t2}\right) \tag{3}$$
$$+2d_sK_{2x}\left(2\Psi_c - X_{t1} - X_{t2}\right) = L_b[F_{y1} - F_{y2}]$$

2.1.2 Bogie dynamics (i =1,2)

$$M_t\ddot{y}_{ti} + 2c_{1y}\left[2\dot{y}_{ti} - \left(\dot{y}_{w(2i-1)} + \dot{y}_{w(2i)}\right) + 2h_1\dot{\theta}_{ti}\right]$$
$$+2c_{2y}\left[\left(\dot{y}_{ti} - \dot{y}_{w(2i-1)}\right) - \left(h_3\dot{\theta}_c + h_2\dot{\theta}_{ti}\right) - (-1)^iL_b\dot{\Psi}_c\right]$$
$$+\ 2k_{1y}\left[2y_{ti} - \left(y_{w(2i-1)} + y_{w(2i)}\right) + 2h_1\theta_{ti}\right] \tag{4}$$
$$+2k_{2y}\left[\left(y_{ti} - y_c\right) - \left(h_3\theta_c + h_2\theta_{ti}\right) - (-1)^iL_b\Psi_c\right] = -F_{yi}$$

$$J_{xt}\ddot{\theta}_{ti} + 2h_1c_{1y}\left[2h_1\dot{\theta}_{ti} + \left(2\dot{y}_{ti} - \left(\dot{y}_{w(2i-1)} + \dot{y}_{w(2i)}\right)\right)\right]$$
$$+2h_2c_{2y}\left[h_3\dot{\theta}_c + h_2\dot{\theta}_{ti} + \left(\dot{y}_{ti} + \dot{y}_c\right) - (-1)^iL_b\dot{\Psi}_c\right]$$
$$+2b^2{}_1c_{1z}\left[2\dot{\theta}_{ti} - \left(\dot{\theta}_{w(2i-1)} + \dot{\theta}_{w(2i)}\right)\right]$$
$$+2b^2{}_2c_{2z}\left[\dot{\theta}_{ti} - \dot{\theta}_c\right] + 2h_1k_{1y}\left[2h_1\theta_{ti} + \left(2Y_{ti} - \left(Y_{w(2i-1)} + Y_{w(2i)}\right)\right)\right] \tag{5}$$
$$+2h_2k_{2y}\left[h_3\theta_c + h_2\theta_{ti} + \left(Y_{ti} + Y_c\right) - (-1)^iL_b\Psi_c\right] + 2b^2{}_1k_{1z}\left[2\theta_{ti} - \left(\theta_{w(2i-1)} + \theta_{w(2i)}\right)\right]$$
$$+2b^2{}_2k_{2z}\left[\theta_{ti} - \theta_c\right] = -F_{yi}h_3$$

$$J_{Zt}\ddot{\Psi}_{ti} + 2d^2{}_pc_{1x}\left[2\dot{\Psi}_{ti} - \left(\dot{\Psi}_{w(2i-1)} + \dot{\Psi}_{w(2i)}\right)\right]$$
$$+2L_dc_{1y}\left[2L_d\dot{\Psi}_{ti} - \left(\dot{Y}_{w(2i-1)} - \dot{Y}_{w(2i)}\right)\right] + 2d^2{}_pk_{1x}\left[2\Psi_{ti} - \left(\Psi_{w(2i-1)} + \Psi_{w(2i)}\right)\right] \tag{6}$$
$$+2d^2{}_sk_{2x}\left[\Psi_{ti} - \Psi_c\right] + 2L_dk_{1y}\left[2L_d\theta_{ti} - \left(Y_{w(2i-1)} - Y_{w(2i)}\right)\right] = 0$$

2.1.3 Wheel-set dynamics (i =1,2, while j =1; i =3,4, while j =2)

$$
\begin{aligned}
&M_w \ddot{y}_{wi} + 2c_{1y}\left[\left(\dot{Y}_{wi} - \dot{Y}_{tj}\right) - h_1\dot{\theta}_{tj} + (-1)^i L_d \dot{\Psi}_{tj}\right] \\
&+2k_{1y}\left[\left(Y_{wi} - Y_{tj}\right) - h_1\theta_{tj} + (-1)^i L_d \dot{\Psi}_{tj}\right] + k_{gy}\left[Y_{wi} - Y_{ai} - R_1\theta_{cli}\right] \\
&+2 f_{22}\left[\frac{1}{V}\left(1 + \frac{\sigma R_1}{a}\right)\dot{Y}_{wi} - \frac{\sigma R_1}{V a}\dot{Y}_{ai} - \frac{\sigma R_1^2}{V a}\dot{\theta}_{cli} - \Psi_{wi}\right] = 0
\end{aligned}
\tag{7}
$$

$$
\begin{aligned}
&J_{Zw}\ddot{\Psi}_{wi} + 2d_p^2 c_{1x}\left[\left(\dot{\Psi}_{wi} - \dot{\Psi}_{tj}\right)\right] + 2d_p^2 k_{1x}\left[\Psi_{wi} - \Psi_{tj}\right] \\
&+2 f_{11}\left[\frac{\lambda_e a}{R_1}\left(Y_{wi} - Y_{ai} - R_1\theta_{cli}\right) + \frac{a^2}{V}\dot{\Psi}_{wi}\right] + k_{gy}\Psi_{wi} = 0
\end{aligned}
\tag{8}
$$

The definitions and values of various parameters used in equations (1)–(8) are given in Appendix 1, which are the same as in Singh et al. (2017). The state space formulation of the above system is given in the next section.

2.2 State-space formulation

Let,

$q = [Y_c, \theta_c, \psi_c, Y_{t1}, \theta_{t1}, \psi_{t1}, Y_{t2}, \theta_{t2}, \psi_{t2}, Y_{w1}, \psi_{w1}, Y_{w2}, \psi_{w2}, Y_{w3}, \psi_{w3}, Y_{w4}, \psi_{w4}]^{\mathrm{T}}$,

$u = [F_{y1}, F_{y2}]^{\mathrm{T}}$, and

$w = [Y_{a1}, Y_{a2}, Y_{a3}, Y_{a4}, \theta_{cl1}, \theta_{cl2}, \theta_{cl3}, \theta_{cl4}\ \dot{Y}_{a1}, \dot{Y}_{a2}, \dot{Y}_{a3}, \dot{Y}_{a4}, \dot{\theta}_{cl1}, \dot{\theta}_{cl2}, \dot{\theta}_{cl3},$

$\dot{\theta}_{cl4}]^{\mathrm{T}}$ be defined the displacements (linear and angular), control, and disturbance vectors, respectively.

Then the equations of motion, represented by equations (1)–(8) can be written in the following matrix form

$$
[M]\ddot{q} + [C]\dot{q} + [K]q = [F_u]u + [F_w]w \tag{9}
$$

where [M] ($\mathcal{R}^{17\times17}$), [C] ($\mathcal{R}^{17\times17}$), and [K] ($\mathcal{R}^{17\times17}$) are the mass, damping, and stiffness matrices of the vehicle system; $[F_u]$ ($\mathcal{R}^{17\times2}$), $[F_w]$ ($\mathcal{R}^{17\times16}$) are the position matrices of control inputs and track disturbances acting on the railway vehicle body and wheels of wheelsets.

$$
\begin{cases}
\dot{x} = [A]x + [B_1]u + [B_2]w \\
y = [C]x + [D_1]u + [D_2]w
\end{cases}
\tag{10}
$$

Now by defining the state vector as $\dot{x} = [q^{\mathrm{T}}\dot{q}^{\mathrm{T}}]^{\mathrm{T}}$, the state and output equations of the railway vehicle system in the form of state-space are given as

where

$$[A]=\begin{bmatrix}0 & \mathrm{I}\\ -M^{-1}K & -M^{-1}C\end{bmatrix}\in\mathcal{R}^{34\times34},\ [B_1]=\begin{bmatrix}0\\ M^{-1}F_u\end{bmatrix}\in\mathcal{R}^{34\times2},$$

$$\text{and}\,[B_2]=\begin{bmatrix}0\\ M^{-1}F_w\end{bmatrix}\in\mathcal{R}^{34\times16},$$

are the system, control, and disturbances matrices, respectively. $[C]=\begin{bmatrix}-M^{-1}K & -M^{-1}C\end{bmatrix}\in\mathcal{R}^{17\times34}$ is the output matrix with $[D_1]=\begin{bmatrix}M^{-1}F_u\end{bmatrix}\in\mathcal{R}^{17\times2}$, and $[D_2]=\begin{bmatrix}M^{-1}F_w\end{bmatrix}\in\mathcal{R}^{17\times16}$ are the transfer matrices, respectively. The values of all coefficient matrices can be derived from equation (9).

3 Validation of the proposed model with experimental results

The results of the proposed analytical model of LHB-FIAT coach with passive suspension are validated using the oscillations test experiment results (Indian Railway Technical Bulletin, 2013). In particular, RDSO conducted the test trials on a prototype LHB chair car (as shown in Figure 2(a)) to evaluate the ride comfort in a test speed range of 33.33–50 m/s (120–180 Km/h). In the measurement, accelerometers and displacement sensors are connected by a cable to the data acquisition system in the equipment cabin. During oscillation test trials, these sensors record acceleration and displacement signals on the wheelset axle-box, the car body's floor, and the test coach's bogie frame. RDSO/Sperling's criteria that were used to evaluate the ride index of coaches equipped with coil springs in the secondary suspensions is elaborated in the following section.

3.1 Sperling's method

To evaluate the ride comfort of passengers, W_z (Ride factor) is introduced by Sperling is used (Dumitriu and Gheti, 2016). In this method, the vehicle itself plays the role of judge. Here the ride comfort implies that the vehicle is to be assessed according to the effect of mechanical vibration on the occupants.

The evaluation scale used for determining ride comfort is given in Table 2. Since the acceleration spectrum is a continuous function of frequency, therefore W_z is also a continuous function of frequency and is obtained by integration over the frequency interval of the human sensitivity range, i.e., 0–30 Hz. The following equation can be used to find the comfort index W_z in the frequency domain.

$$W_z=\sqrt[10]{\int_{0.5}^{30}a_0{}^3B_s{}^3\mathrm{d}\omega}\tag{11}$$

where a_0 is the acceleration amplitude, and B_w and B_s are the frequency weighting functions determined as:

For lateral motion

$$B_w(f)=0.737\sqrt[2]{\frac{1.911\,(2\pi f)^2+(0.25\,(2\pi f)^2)^2}{(1-0.277\,(2\pi f)^2)^2+(1.563\,(2\pi f)-0.0368\,(2\pi f)^3)^2}}\tag{12}$$

Table 2 Ride evaluation scale

Ride index (W_z)	*Comfort* (*vibration sensitivity*)
1	Just noticeable
2	Clearly noticeable
2.5	More pronounced but not unpleasant
3	Strong, irregular, but still tolerable
3.25	Very irregular
3.5	Extremely irregular, unpleasant, annoying; prolonged exposure intolerable
4	Extremely unpleasant; prolonged exposure intolerable

The experimental and simulated implementation of riding performance in the lateral directions at a speed of 160, 170, and 180 km/h under loaded and tare conditions have been shown in Figure 2(b) and (c). Additionally, it should be noted that the values produced using the suggested model show greater agreement with the experimental data, with error ranges of 2.36–8.81% under tare condition and 5.84–8.30% under loaded condition.

Figure 2 (a) Field test photo of prototype LHB chair car and comparison of experimental and simulated ride comfort index under; (b) tare condition and (c) loaded condition (see online version for colours)

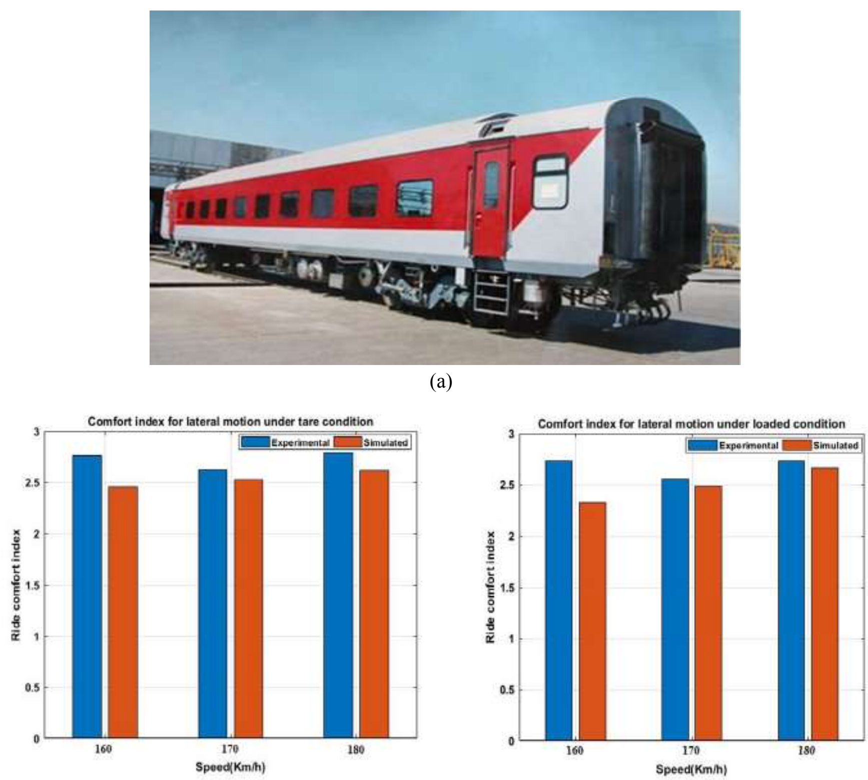

(a)

(b) (c)

4 Track irregularities model

The leading cause of vibrations in the railway's vehicle body is the irregularities on railway tracks and wheel structure (Wang et al., 2019). These irregularities act as input excitation to the railway vehicle. There are three types of track irregularity, such as vertical profile (Z_r), lateral alignment (Y_a), and cross-level (θ_{cl}) are defined in the literature (Goodwin, 1987), which excite the vehicle's body in vertical and lateral directions. Out of which, alignment and cross-level are the primary cause of lateral vibrations. These irregularities can be periodic as well as random in nature.

4.1 Periodic track irregularities

The track irregularities can be broken down into harmonic components with the help of a Fourier transformation, in which the wavelengths possess special significance. At a particular speed and direction, the car body's lateral, roll, and yaw motion is excited by some wavelengths, as shown in Figure 3. These wavelengths can be described as 'critical wavelengths" for the speed (Lewis and Olofsson, 2006). According to this, the sinusoidal or periodic input function used for lateral motion is defined as

$$Y_a(t) = A_o \sin\left(2\pi \frac{V}{l_1} t\right) \tag{13}$$

where V is the velocity of the vehicle. A_o is the amplitude, and l_1 is the spatial wavelength for lateral motion, respectively, as shown in Figure 3(a).

Figure 3 Track irregularities (a), (b) lateral alignment, (c) cross-level

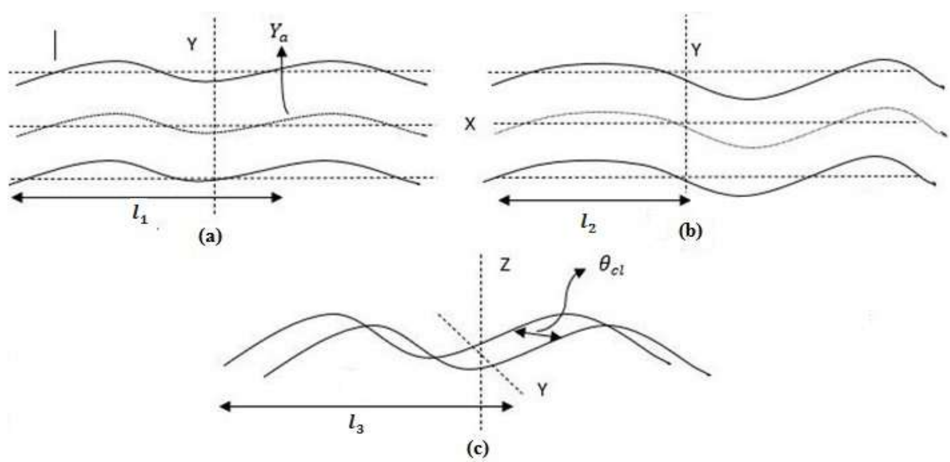

Similarly, the input function used for yaw motion is defined as:

$$Y_a(t) = A_o \sin\left(2\pi \frac{V}{l_2} t\right) \tag{14}$$

where l_2 represents the spatial wavelength for yaw motion, respectively, as shown in Figure 3(b).

And a different input function is used for roll motion which is defined as:

$$\theta_{cl}(t) = A_o \sin(2\pi \frac{V}{l_3} t) \tag{15}$$

where, l_3 is the spatial wavelength for roll motion as shown in Figure 3(c).

If Y_a, and θ_{cl} are the excitations applied on the front wheelsets of railway vehicle, then $Y_{a1} \sim Y_{a4}$, and $\theta_{cl1} \sim \theta_{cl4}$ are related by the following relation

$$\begin{cases} Y_{a2} = Y_a(t-\tau_1), Y_{a3} = Y_a(t-\tau_2), Y_{a4} = Y_a(t-\tau_3) \\ \theta_{cl2} = \theta_{cl}(t-\tau_1), \theta_{cl3} = \theta_{cl}(t-\tau_2), \theta_{cl4} = \theta_{cl}(t-\tau_3) \end{cases} \tag{16}$$

where $\tau_1 = \frac{2L_d}{V}$, $\tau_2 = \frac{2L_b}{V}$, $\tau_3 = \frac{2(L_d + L_b)}{V}$ are the time delays between the front and consecutive wheelsets.

4.2 Random track irregularities

The actual track irregularities are the superposition of harmonic waves of different amplitude, phase, and wavelength. Describing the random track irregularities is always convenient in the form of power spectral density (PSD), as given in equations (17) and (18), which are calculated by taking the Fourier Transform of the autocorrelation function as given in (Wanming Zhai, 2020).

$$S_a(\omega) = \frac{A_a \,.\, \Omega_c^2 \,.\, V^3}{\left(\omega^2 + (V.\,\Omega_r)^2\right)\left(\omega^2 + (V.\,\Omega_c)^2\right)} \frac{m^2}{(\frac{rad}{sec})} \tag{17}$$

$$S_{cl}(\omega) = \frac{A_v \,.\, \Omega_c^2 \,.\, V^3 .\, \omega^2}{l_r^2\left(\omega^2 + (V.\,\Omega_r)^2\right)\left(\omega^2 + (V.\,\Omega_c)^2\right)\left(\omega^2 + (V.\,\Omega_s)^2\right)} \frac{m^2}{\left(\frac{rad}{sec}\right)} \tag{18}$$

where ω is the angular frequency of the track measured in rad/sec and Ω_r, Ω_c and Ω_s are the cut-off frequencies taken in rad/m; A_v, A_a are roughness constant taken in $m^2.\frac{rad}{m}$; V is the velocity of the vehicle; l_r is half the distance between the two-rolling circle of the wheelset (m). The values of these constant factors and cut-off frequencies for different classes of track are given in Table 3.

Table 3 Roughness coefficients and cut-off frequencies for German track irregularities PSDs

Track class	Ω_c (rad/m)	Ω_c (rad/m)	Ω_c (rad/m)	A_a (m^2. rad/m)	A_v (m^2. rad/m)
Low	0.8246	0.0206	0.4380	2.119×10^{-7}	4.032×10^{-7}

5 Control scheme and structure

In this paper, a multi-loop or decentralised control structure is developed to suppress the vibrations of the railway vehicle, as illustrated in Figure 4. The developed control structure comprises three optimally tuned FOPID controllers that operate diagonally and work independently to control the lateral, roll, and yaw motion of vehicle body. Based on the error and command signal, the above three body motions are controlled by implementing two actuators. These two actuators are mounted horizontally above the front and rear bogies, which controls the vehicle body's lateral, roll, and yaw motion, as demonstrated in equation (19).

$$\begin{cases} Above\ front\ bogie\ actuator = Lateral(u_1) + roll\ (u_2) + yaw(u_3) \\ Above\ rear\ bogie\ actuator = Lateral(u_1) + roll\ (u_2) - yaw(u_3) \end{cases} \tag{19}$$

Figure 4 Decentralised control structure for railway vehicle

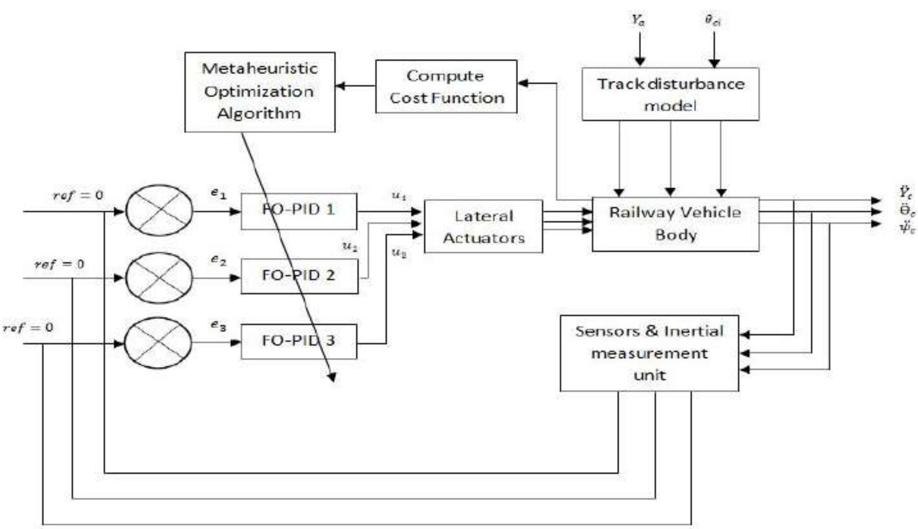

6 Controller and optimisation algorithms

This section describes the proposed FOPID controller and the different algorithms tuning the controller parameters.

6.1 FO-PID controller

Over the last decade, fractional calculus applications have shown a significant impact in the field of Engineering and Mathematics. Leibniz and L'Hospital, in 1695, first coined the idea of fractional calculus. Since then, fractional calculus has been an ongoing research area. Its applications in control engineering have attracted many researchers because fractional order differential equations better characterise real-world physical systems. Recent research studies show that fractional order controllers perform better than integer order controllers in terms of system performance and robustness. Fractional calculus is the main foundation of FOPID. Here, the differentiation and integration operations are collaboratively used in fractional order. The continuous form of integral-differential is defined as:

$$\alpha\mathcal{D}_t^s = \begin{cases} \dfrac{ds}{dt} & R(s) > 0 \\ 1 & R(s) = 0 \\ \int_{\infty}^{t} \mathrm{d}\tau^{-s} & R(s) < 0 \end{cases} \tag{20}$$

where s is the order of operation, α and t are the confines of operation. Fractional calculus empowers the derivative and integral to be in non-integer order. There are several definitions available for fractional integral-differential operation.

In the fractional order PID, the integral-differential equation which defines the control action of the controller can be expressed as:

$$U(t) = K_P e(t) + K_I D^{-\lambda} e(t) + K_D D^{\mu} e(t) \tag{21}$$

Applying Laplace transform to equation (21), the control action of the FOPID controller is expressed in terms of the transfer function as:

$$C(s) = \frac{U(s)}{E(s)} = K_P + K_I s^{-\lambda} + K_D s^{\mu}\text{ , }(\lambda,\ \mu > 0) \tag{22}$$

where,

- $C(s)$ is the controller transfer function
- $E(s)$ is the error
- $U(s)$ is the output
- K_P, K_I and, K_D are the controller proportional, integral, and derivative gains
- λ is the order of integration
- μ is the order of differentiation.

The fractional order PID is an extended version of integer PID achieved by fractional-ordering the integral and derivative action, i.e., the FOPID is a sum of fraction operators, along with controller gains. From equations (21) and (22), it can be seen that FOPID has two more parameters (such as λ and μ) as compared to conventional PID, which provides additional flexibility in designing the control system. Also, the involvement of the two more controller parameters shows that the design procedure of FOPID consists of five nonlinear equations to be solved. The complexity of these five nonlinear equations is very significant, mainly because of the fraction orders. Considering the difficulties, MATLAB, with a suitable tool, could be a better choice for designing the controller. The proposed system's controller design uses the FOMCON toolbox with Oustaloup's analytical approximation technique described in Baranowski et al. (2015) and Lanusse et al. (2015).

Many tuning methods are available for these five parameters, generally named rule-based, numerical, and analytical. Here, the following methods are used for tuning the optimum parameters of FOPID.

6.2 Optimisation algorithms

6.2.1 Ziegler-Nichols (Z-N) method

To tune the FOPID parameters, firstly, the modified form of the Z-N method proposed by Duarte Valerio et al. (Valério and da Costa, 2006) has been implemented, which comes under rule-based methods. The tuning rules of FO-PID are similar to that of conventional PID. Here, the step response of the plant assumes to have an S-shaped curve, as shown in Valério and da Costa (2006). From the curve, depending upon the value of L and T, two sets of tuning are established, given in Table 4, where L denotes the delay and T can be interpreted as the time constant. Here P (proportional gain) can be read as:

$$P = -0.0048 + 0.2664L + 0.4982T + 0.0232\,L^2 - 0.0720\,T^2 - 0.0348LT$$

And so on

Table 4 Modified Ziegler Nichols parameters

Parameters to use when $0.1 \le T \le 5$					
	P	I	λ	D	μ
1	–0.0048	0.3254	1.5766	0.0662	0.8736
L	0.2664	0.2478	–0.2098	–0.2528	0.2746
T	0.4982	0.1429	–0.1313	0.1081	0.1489
L^2	0.0232	–0.1330	0.0713	0.0702	–0.1557
T^2	–0.0720	0.0258	0.0016	0.0328	–0.0250
LT	–0.0348	–0.0171	0.0114	0.2202	–0.0323
Parameters to use when $5 \le T \le 50$					
	P	I	λ	D	μ
1	2.1187	–0.5201	1.0645	1.1421	1.2902
L	–3.5207	2.6643	–0.3268	–1.3707	–0.5371
T	–0.1563	0.3453	–0.0229	0.0357	–0.0381
L^2	1.5827	–0.1094	0.2018	0.5552	0.2208
T^2	0.0025	0.0002	0.0003	–0.0002	0.0007
LT	0.1824	–0.1054	0.0028	0.2630	–0.0014

The parameters obtained from these rules can be used as an excellent initial guess for the metaheuristic optimisation algorithms discussed below.

6.2.2 Particle swarm optimisation (PSO) algorithm

In recent years, the PSO algorithm has emerged as a potential tool for solving a wide range of problems in control engineering. The PSO algorithm uses the nature-inspired mechanism of bird flocking or fish schooling with a targeted position in searching for potential food. Kennedy et al. (Slowik, 2011) proposed this algorithm in 1995, which uses the actions of swarm intelligence in which each particle focuses on finding the potential solution according to the given objective function. Each particle reaches its best position according to experience and awareness of the neighbouring particle they are going through. Due to its diverse nature, such as by changing its parameters and population size, PSO can be easily used with other heuristic algorithms. It uses in various kinds of applications, such as medicines (Eshtay et al., 2018), financial studies (Shie et al., 2012), structural studies (Hajihassani et al., 2018), communication engineering (Ganguly et al., 2010), and automatic control systems (Chang and Chen, 2014). In the control system, PSO is mainly used to solve the single or multi-objective function, which helps to get the desired transient and steady-state responses. The present investigation employed this algorithm to solve a single objective multivariable optimisation problem using for proposed vibration control structure. The pseudo-codes of this algorithm for the presently investigated problem are illustrated in Appendix 2.

6.2.3 Grey wolf optimisation (GWO) algorithm

GWO is a new optimisation technique developed by Mirjalili et al. (2014). The motivation for developing the GWO algorithm is inspired by the intellectual hunting tactics followed by grey wolves. Generally, grey wolves have well-defined groups of 10–12 wolves called packs, and the duty of each wolf in a group is defined in a particular way. It has four levels of hierarchy named alpha (α), beta (β), delta (δ), and omega (ω) that guide the hunting process. The top level of this hierarchy, alpha (α), has a leader who dominates decision-making. The other two levels, beta, and delta, are the sub-ordinates that help the alpha to make the best possible solutions. In addition to this social hierarchy, the hunting of wolves is depicted in the following way: Search or advance the prey; encircle it and restrict its movement; finally, attack and kill the prey. The applications of GWO show tremendous results in the field of machine learning (Al-Tashi et al., 2019; Emary et al., 2016), medical or bioinformatics (Sharma et al., 2020, 2019), image processing (Li et al., 2017), and wireless sensor networks (Rajakumar et al., 2017). However, in recent years there has been an explosion in the publication that explores the use of GWO in control engineering applications (Debnath, 2016; Ren et al., 2022; Sule et al., 2020). In this paper, we use this algorithm to tune the five parameters of the FOPID controller that helps to achieve the desired output response. The pseudo-code of this algorithm used for the proposed control scheme is illustrated in Appendix 2.

6.2.4 Hybrid PSO-GWO algorithm

The metaheuristic algorithms work on the principle of randomisation, which employs a particular mix of local and global searches generally known as exploration and exploitation. Heuristics and metaheuristics are not defined in a way that can be checked or used as a standard. However, these techniques show significant results within a reasonable time by providing the optimum solution for integer order or less dimensional systems. But when it comes to the non-integer or higher dimensional world, it may get trapped into local minimum points and can take ample time to provide the optimum solution. Therefore to address these problems, a novel hybrid PSO-GWO optimisation algorithm is proposed, which uses a diverse search strategy that balances the local and global searches. Also, the problem of higher dimensionality is reduced in the case of the hybrid algorithm as the three parameters (K_p, K_I, and K_D) of the FOPID controller are tuned with the help of PSO, and the other two parameters (λ and μ) are tuned with GWO. The functional flow diagram of hybrid PSO-GWO has been illustrated in Figure 5.

Figure 5 Workflow diagram of hybrid PSO-GWO

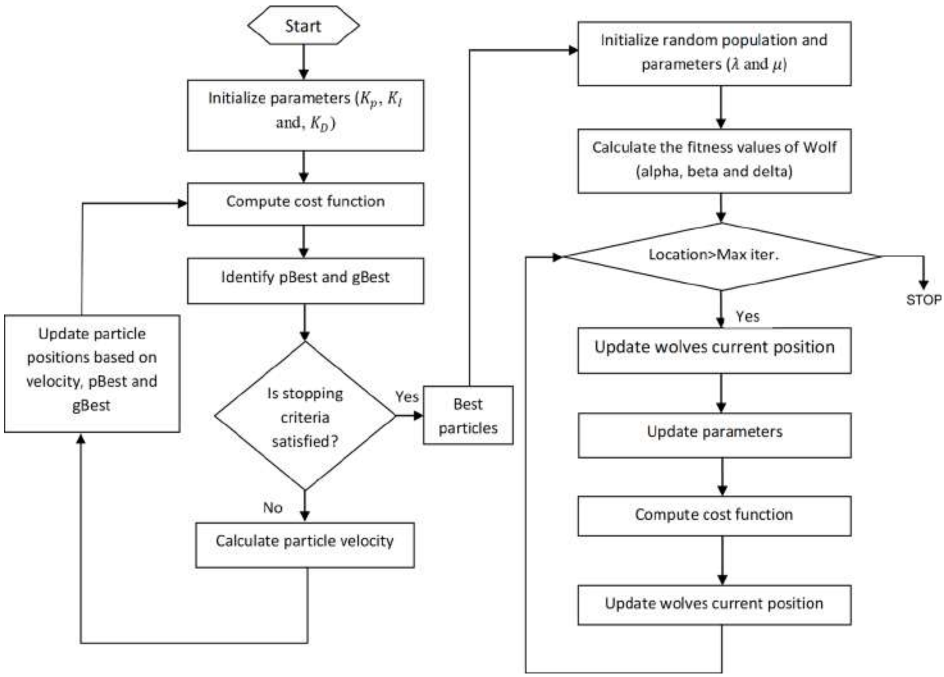

7 System response based on a decentralised control structure

In order to achieve better ride comfort, the acceleration response of the vehicle body in translational as well as rotational motion should be minimised. Thus, from equation (10), the controlled outputs are defined as

$$[y_o] = [\ddot{Y}_c, \ddot{\psi}_c, \ddot{\varnothing}_c] \tag{23}$$

The relation between the first and last set of wheelsets is defined in equation (16). Therefore, based on this, let $n = [Y_{a1},\ \theta_{cl1},\ \dot{Y}_{a1},\ \dot{\theta}_{cl1}]^{\mathrm{T}} \cong [Y_a,\ \theta_{cl},\ \dot{Y}_a,\ \dot{\theta}_{cl}]^{\mathrm{T}}$ and $\hat{G}_{wn}(\mathrm{s}) = \left[1,\ \mathrm{e}^{-\tau_1 \mathrm{s}},\ \mathrm{e}^{-\tau_2 \mathrm{s}},\ \mathrm{e}^{-\tau_3 \mathrm{s}}\right]^{\mathrm{T}}$, Then we have

$$N(s) = G_{wn} W(s) \tag{24}$$

where $G_{wp} = diag\ \{\hat{G}_{wn}(\mathrm{s}),\ \hat{G}_{wn}(\mathrm{s}),\ \hat{G}_{wn}(\mathrm{s}),\ \hat{G}_{wn}(\mathrm{s})\}$

Thus, from equations (10), (23), and (24), the two transfer function matrix, i.e., between the inputs and outputs of the system, can be evaluated as

$$P(s)=\begin{bmatrix} p_{11}(s) & \cdots & p_{1n}(s) \\ \vdots & \ddots & \vdots \\ p_{n1}(s) & \cdots & p_{nn}(s) \end{bmatrix};\ G(s)=\begin{bmatrix} g_{11}(s) & \cdots & g_{1n}(s) \\ \vdots & \ddots & \vdots \\ g_{n1}(s) & \cdots & g_{nn}(s) \end{bmatrix} \tag{25}$$

where, $[P(s)]^{n\times n}$ represents the disturbance transfer function matrix having n no. of disturbance inputs and n no. of outputs, and $[G(s)]^{n\times n}$ is a system transfer function matrix having n no. of control inputs and n no. of outputs.

Now, for a $n\times n$ control system, where the interaction between the various control loop is mild, in that case, the transfer function matrix for the decentralised controller can be represented as

$$C(s)=\frac{U(s)}{E(s)}=\begin{bmatrix} c_{11}(s) & 0 & \dots & 0 \\ 0 & c_{22}(s) & \dots & 0 \\ \vdots & \vdots & \vdots & \vdots \\ 0 & 0 & \dots & c_{nn}(s) \end{bmatrix} \tag{26}$$

The single-loop structure of the regulatory feedback system is shown in Figure 6. The closed-loop transfer function between the input and output is

$$T(s)=\frac{Y(s)}{W(s)}=[1+p(s)c(s)g(s)]^{-1}p(s) \tag{27}$$

Likewise, the overall transfer function matrix of the decentralised control system can be written as follows:

$$\begin{aligned} &H(s)=diag[(1+p_{11}(s)c_{11}(s)g_{11}(s)]^{-1}p_{11}(s)); \\ &(1+p_{22}(s)c_{22}(s)g_{22}(s)]^{-1}p_{22}(s)),\ldots, \\ &(1+p_{nn}(s)c_{nn}(s)g_{nn}(s)]^{-1}p_{nn}(s))] \end{aligned} \tag{28}$$

Figure 6 Single loop structure of regulatory feedback system

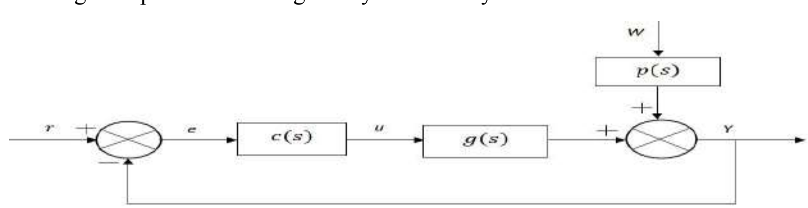

Now, if $H_{nn}(\omega)$ is considered as frequency response function due to harmonically varying input of unit amplitude having frequency response function $W_n(\omega)$ for n^{th} input with all other input kept at zero. Then output and input of the system in the frequency domain are related by the relation as

$$Y_n(\omega) = H_{nn}(\omega) \times W_n(\omega) \tag{29}$$

In the case of random input, the input is considered in terms of PSD, as stated above in equations (15) and (16). For the output response, according to the frequency response analysis (FRA) method, the output mean square spectral density $S_y(\omega)$ is related to input mean square spectral density $S_n(\omega)$ by the following relation

$$S_y(\omega) = |H_{nn}(\omega)|^2 \times S_n(\omega) \tag{30}$$

where,

$$H_{nn}(\omega) = \frac{1}{1 - \left(\dfrac{\omega}{\omega_n}\right)^2 + j2\zeta_n\left(\dfrac{\omega}{\omega_n}\right)} \tag{31}$$

where $\left(\dfrac{\omega}{\omega_n}\right)$ is the normalised frequency, and ζ is the damping ratio.

Then finally, the RMS acceleration response is calculated as:

$$a_0 = \sqrt{\int_{\omega 1}^{\omega 2} \omega^4 . S_n(\omega) d\omega} \tag{32}$$

8 Results and discussions

This section thoroughly evaluates the performance of FOPID based active suspension control system used for vibration mitigation of railway vehicles. The effectiveness of the controller tuned with metaheuristic optimisation algorithms was investigated in the time and frequency domain under periodic and random track disturbances, respectively. A comparison was conducted between the proposed FOPID control with the Z-N, PSO, GWO, and hybrid PSO-GWO tuning strategies. The improvement of proposed control schemes over the passive system was evaluated based on the following proposed quadratic cost function.

$$J = \frac{1}{2}\int_0^{t_f} r_1 . \ddot{x}_{max}^{2} + r_2 . y_{max}^2 \tag{33}$$

where $\ddot{x}$ and y represent the maximum accelerations (ms^{-1}) and maximum control efforts (N) of respective controlling states. According to the cost function, the lateral, roll, and yaw motions of the vehicle body can be regulated by changing the values of the coefficient sr_1, and r_2. The appropriate choices of the coefficients for translational and angular motion have been provided in Table 5. The various parameters of railway vehicle, and track used in this study have been given in Appendix 1. The simulation has been done in MATLAB/SIMULINK environment using the FOMCON toolbox with a maximum step size of 1e-3.

Table 5 Different values of coefficients used in the cost function

Motions	r_1	r_2
Lateral	0.030	1000
Roll	0.030	1500
Yaw	0.030	1500

The performance of an optimisation-based FOPID controller depends on how well the controller parameters are tuned within the constraints of the required objective function, which ultimately depends on the specific range of controller parameters. Thus, by taking the classical approach (Z-N) as training optimum parameters, this method can provide an excellent initial guess for controller parameters and be a benchmark in designing the FOPID with the other three metaheuristic techniques. The parameters required for implementing the proposed optimisation techniques have been demonstrated in the *Psuodo code* (Appendix 2). Each algorithm has been run ten times by setting the same number of iterations, particles, and other parameters of PSO, GWO, and hybrid PSO-GWO. Then, the best convergence graphs to find the optimum values of the FOPID controller using these techniques have been given in Figure 7. Also, the best optimum FOPID parameters (K_p, K_p, K_p, λ, μ), and the corresponding cost function (O_f) values for lateral, roll, and yaw motion, results from classical and metaheuristic tuning have been provided in Table 6. Figure 7 shows that although the convergence rate of PSO and GWO is substantially faster than the hybrid PSO-GWO, they have the problem of being trapped in local minima, as demonstrated in Figures 7(b) and (c) do not guarantee an optimum solution. On the other hand, despite the rate of convergence of hybrid PSO-GWO being slower than PSO, GWO; it still performs better for minimisation of the cost function (O_f) as illustrated in Table 6, and also does not have the problem of getting trapped into local minimum points, which shows the efficacy of the proposed algorithm over PSO and GWO.

8.1 Simulation under periodic track irregularities

8.1.1 Time domain responses of acceleration of the body

The first harmonic periodic functions are used as input disturbances to check the performance of an optimally tuned FOPID controller with metaheuristic algorithms. Let the parameters A_o, l_1, l_2, l_3 and V in equations (13)–(15) be 0.01 m, 18 m, 9 m, 18 m and $50\ \mathrm{ms}^{-1}$, respectively, which implies that the fundamental frequency ($\omega = \frac{2\pi V}{l}$) for lateral and roll motion equals $17.45\ \mathrm{rad\ s}^{-1}$, and for yaw motion, equal $8.72\ \mathrm{rad\ s}^{-1}$. The time histories of open-loop output responses and the FOPID-tuned closed-loop responses for the accelerations of the vehicle body in all three modes (lateral, roll, and yaw) have been illustrated in Figure 8. Also, the RMS values, and the percentage improvement of RMS value of lateral, roll and yaw acceleration over passive system (open loop) are given in Table 7. The percentage improvement of RMS values using different tuning algorithms over the passive system has been calculated by using the following equation

$$\%\text{improvement of RMS} = \frac{p_s - c_s}{p_s} \times 100 \tag{34}$$

where p_s and c_s are the RMS values of the passive system and different FOPID-tuned control systems, respectively.

Figure 7 Convergence curves for: (a) lateral; (b) roll and (c) yaw motions (see online version for colours)

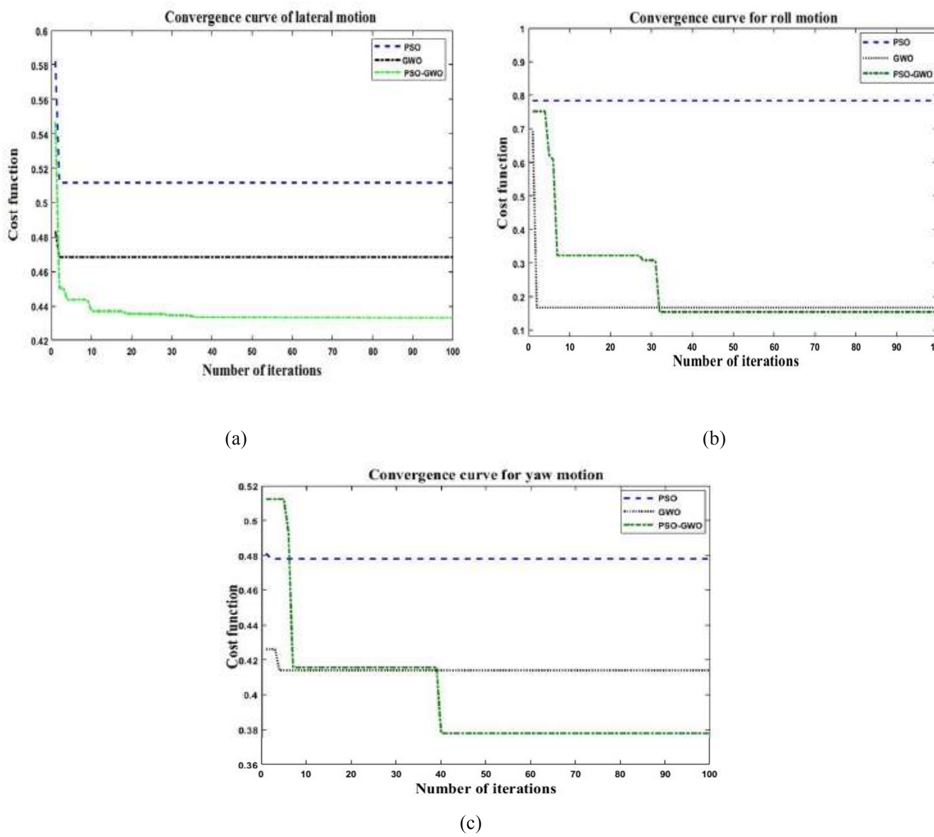

Table 6 FOPID parameters and cost function values resulted from different tuning algorithms

(*a*) *For lateral motion*						
index	K_P	K_D	K_I	λ	μ	O_f
Open loop	–	–	–	–	–	–
Z – N	3.256e+03	7.801e+03	1.064e+04	0.015	0.072	–
PSO	2.716e+04	1.653e+04	2.224e+04	0.051	1.035	0.517
GWO	2.072e+04	3.273e+04	2.626e+04	0.114	0.575	0.477
PSO – GWO	**4.273e+04**	**4.736e+04**	**1.635e+03**	**0.293**	**0.495**	**0.438**
(*b*) *For roll motion*						
index	K_P	K_D	K_I	λ	μ	O_f
Open loop	–	–	–	–	–	–
Z – N	1.205e+04	3.011e+04	1.836e+04	0.052	0.074	–
PSO	2.056e+05	4.773e+04	4.263e+04	0.127	0.273	0.795
GWO	5.026e+04	4.544e+04	1.884e+04	0.166	0.174	0.199
PSO – GWO	**4.835e+05**	**6.272e+04**	**3.021e+04**	**0.488**	**0.641**	**0.198**
(*c*) *For yaw motion*						
index	K_P	K_D	K_I	λ	μ	O_f
Open loop	–	–	–	–	–	–
Z – N	1.873e+04	3.403e+04	3.463e+04	0.052	0.081	–
PSO	1.251e+03	6.516e+04	4.557e+05	0.078	1.027	0.480
GWO	1.982e+03	1.057e+05	2.560e+03	0.624	0.205	0.416
PSO – GWO	**2.684e+05**	**3.362e+05**	**5.122e+03**	**0.361**	**0.963**	**0.378**

Table 7 RMS values and % improvements of vehicle body accelerations under periodic track disturbances

(*a*) *For lateral acceleration*					
index	*Open-loop*	*Z-N*	*PSO*	*GWO*	***PSO-GWO***
RMS Values	5.662e-02	2.826e-02	1.414e-02	1.271e-02	**1.256e-02**
% improvement	–	50.08%	75.02%	77.55%	**77.81%**
(b) *For roll acceleration*					
RMS Values	5.445e-03	3.386e-03	2.623e-03	2.848e-03	**1.345e-03**
% improvement	–	37.81%	51.82%	47.64%	**75.29%**
(c) *For yaw acceleration*					
RMS Values	4.380e-03	4.103e-03	2.944e-03	1.862e-03	**1.588e-03**
% improvement	–	6.3%	32.78%	57.48%	**63.74%**

In the case of lateral motion, from Figure 8(a) and Table 7(a), it is observed that the hybrid PSO-GWO technique provides better results over ZN and PSO when compared to the passive system as it can lower the lateral acceleration up to 77.81%, which is greater than the percentages achieved by ZN (50.08%) and PSO (75.02%). However, compared to GWO, the % improvement of RMS values with a hybrid algorithm is almost similar (approx. 77%). From Figure 8(b) and (c), it is worth observing that when compared to a passive control system, the percentage accelerations (RMS) of roll and yaw motion achieved with FOPID controllers employing the proposed hybrid algorithm are reduced by 75.29% and, 63.74%, respectively, which are comparatively more than other tuning methods as shown in Table 7(b) and (c), respectively.

Figure 8 Time histories of vehicle body acceleration under periodic track disturbances: (a) lateral acceleration ($\ddot{Y}_c$) ; (b) roll acceleration ($\ddot{\theta}_c$), and (c) yaw acceleration($\ddot{\varphi}_c$) (see online version for colours)

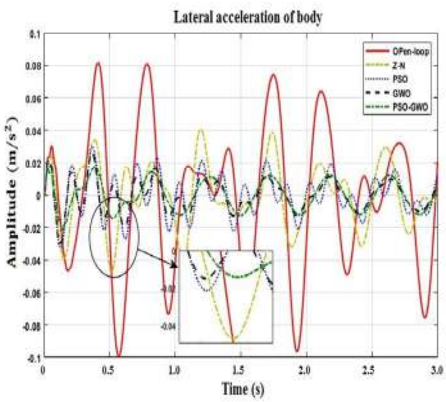

(a)

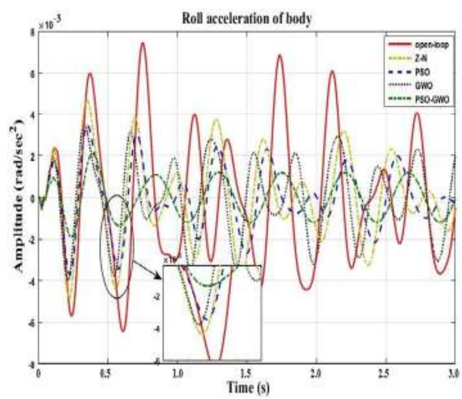

(b)

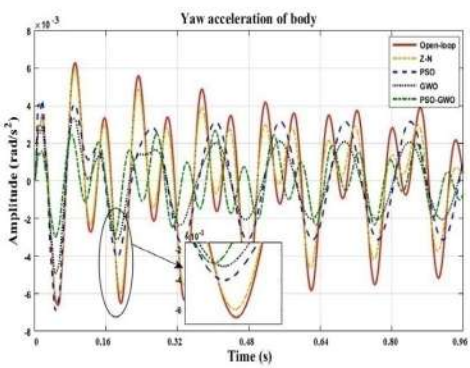

(c)

Now, by using the FOPID controller (20), the control force u could be calculated, which is regarded as the desired force. For the different modes of railway vehicle, the desired force could be achieved with a hydraulic/pneumatic actuator or motor (Wang et al., 2015). Based on equation (19), the time histories of the active force generated by the optimally tuned suspension system to suppress the vibrations of the car body in three modes are shown in Figure 9. Observing Figure 9, it can be seen that the FOPID with hybrid algorithm provides a balanced and optimum actuation force for all modes of vehicle, which satisfies all the parameters of the cost function. Moreover, the FOPID controller satisfies the constraints of maximum force (r_2) in all three modes (given in Table 5) because all the values of the corresponding cost function are less than unity.

From the simulation results shown and discussed in this section, it is observed that the improvement of acceleration of the vehicle body in all three modes using the FOPID controller tuned with three metaheuristic algorithms is remarkable as compared to the passive system and Z-N tuning approach. It is also noticeable that among the three metaheuristic algorithms, the controller tuned with the proposed hybrid PSO-GWO algorithm provides better attenuation than the controller tuned with the other two metaheuristic algorithms.

Figure 9 Time histories of active force for different motions of railway vehicle: (a) lateral motion (u_1); (b) roll motion (u_2) and (c) yaw motion (u_3) (see online version for colours)

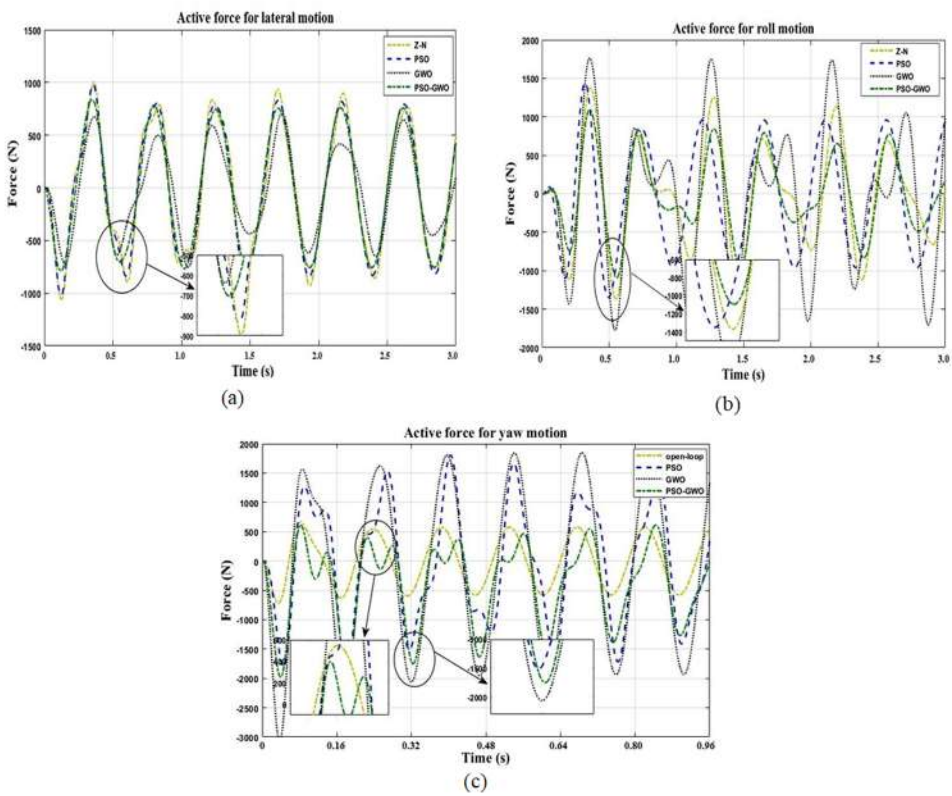

8.2 Simulation under random track irregularities

8.2.1 Frequency domain responses of acceleration of the body

In order to illustrate the efficiency of an optimally tuned FOPID controller in the frequency domain, another track profile known as random excitation input has been considered. Now, using equation (29), the power spectral densities (PSDs) of the vehicle body's lateral, roll, and yaw accelerations calculated from the open loop and closed loop control systems have been given in Figure 10. Also, the RMS values and % improvement of RMS values with different tuning algorithms over the passive system are also provided in Table 8.

Figure 10 Power spectral densities of vehicle body acceleration under random track inputs: (a) lateral acceleration $(\ddot{Y}_c)$; (b) roll acceleration $(\ddot{\theta}_c)$, and (c) yaw acceleration$(\ddot{\varphi}_c)$ (see online version for colours)

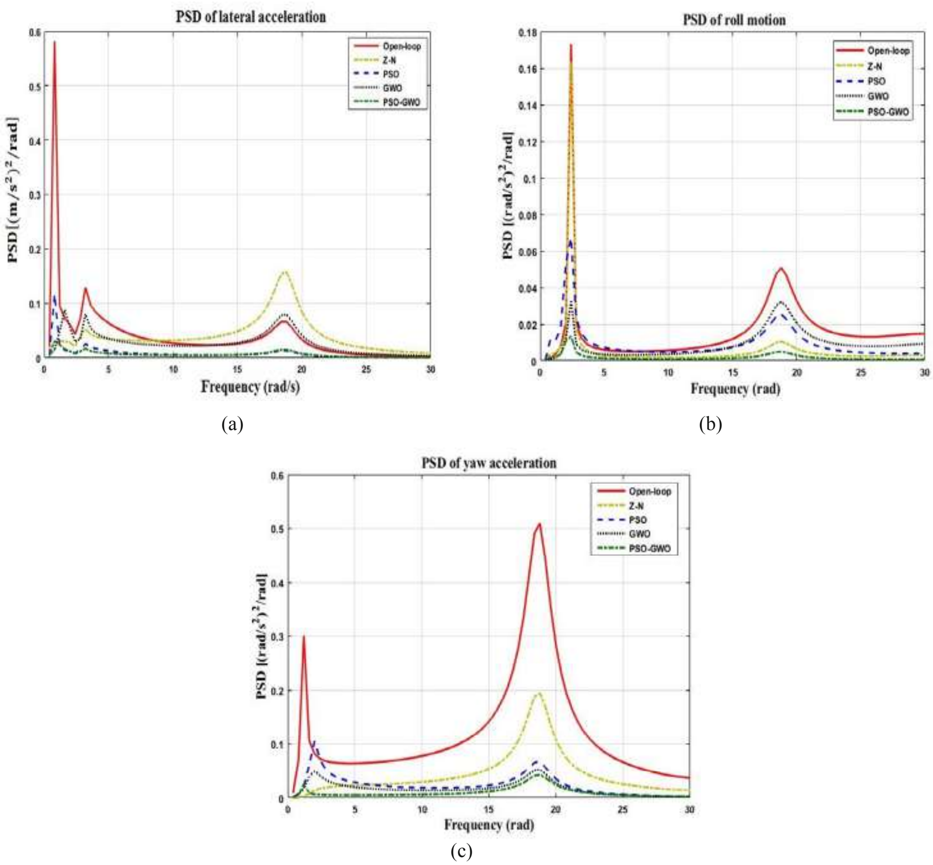

In the case of lateral motion, observing Figure 10(a), it can be seen that the vibration attenuation ability of the ASS for the first and second resonant peaks is good with all tuning algorithms, but for the third resonant peak at the range [17–20] rad/s, ZN and PSO perform worse than GWO and hybrid algorithms. However, among GWO and hybrid algorithms, the performance of the hybrid algorithm retains the good attenuation ability as it can reduce the lateral vibration up to 57.22%, which is more than that of GWO and other tuning techniques shown in Table 8(a).

As for roll acceleration, from Figure 9(b), it is observed that the attenuation ability of the ASS tuned with three metaheuristic algorithms for the first and second resonant peak is superior to that of the passive suspension system and ZN tuning algorithm. Table 8(b) shows that the RMS value of roll acceleration with the hybrid algorithm is lower than that of other tuning methods; the reduction percentage of RMS values is about 77.88%, which is the highest among all the tuning algorithms. Moreover, in the case of yaw motion, from Figure 10(c) and Table 8(c), it is also seen that an ASS controlled with an optimal tuned FOPID controller can reduce the yaw acceleration of the vehicle body by a large extent as compared to the passive system. However, among all tuning methods, hybrid PSO-GWO achieves a 69.58% reduction in RMS values of yaw acceleration. In contrast, the percentage reduction is only 32.35%, 58.71%, and 64.11%, as in the case of ZN, PSO, and GWO. Therefore from these simulation results, we can say that the ride quality of railway vehicles with ASSs controlled with an optimal tuned FOPID controller is significantly improved compared to the passive system.

Table 8 RMS values and % improvement of vehicle body acceleration under random track disturbances

(*a*) *For lateral motion*					
index	*Open-loop*	*Z-N*	*PSO*	*GWO*	***PSO-GWO***
RMS Values	1.221e-02	9.114e-03	7.230e-03	6.824e-03	**5.223e-03**
% improvement	–	25.35%	40.78%	44.11%	**57.22%**
(*b*) *For roll motion*					
RMS Values	6.475e-03	5.582e-03	3.662e-03	1.884e-03	**1.432e-03**
% improvement	–	13.79%	43.44%	70.90%	**77.88%**
(*c*) *For yaw motion*					
RMS Values	4.166e-03	2.818e-03	1.720e-03	1.495e-03	**1.269e-03**
% improvement	–	32.35%	58.71%	64.11%	**69.58%**

9 Conclusions

This work investigates an ASS for a railway vehicle controlled by a FOPID controller and optimised using a hybrid optimisation technique. A 17-DOF dynamic model of a full-scale railway car with wheel-rail forces and the active suspension was created, and its ride comfort results were confirmed using RDSO testing data. Two forms of periodic and random track irregularities, i.e., lateral alignment and cross-level, were used as input. After developing the dynamic model and irregularities methods, a decentralised control system with three independent FOPID controllers was used to suppress the vibration of the car body's motions. A unique hybrid metaheuristic method termed hybrid PSO-GWO was suggested to determine the optimum active force for the suspension system. The simulated results were compared with a passive system, classical (ZN), and two metaheuristic tuning algorithms (PSO, GWO). The car body's lateral, roll, and yaw accelerations under periodic and random track imperfections were investigated in both time and frequency domains. The following outcomes are encased by simulation and analysis:

1 The proposed hybrid algorithm (PSO-GWO) tuned FOPID controller provides the best trade-off between maximum acceleration and control efforts expressed in terms of quadratic cost function compared to PSO and GWO. In contrast, PSO and GWO

have a faster convergence than the proposed hybrid algorithm but have a trapping issue at the local minimum points.

2 Under periodic track disturbances, the time domain controller performance shows a significant decrement in the translational and angular accelerations of the vehicle body relative to the passive system. It was also noted that the suspension system controlled with a hybrid-tuned FOPID controller has comparatively better attenuation towards the vehicle vibration in terms of the percentage improvement in RMS values. It provides approximately 77.81%, 75.29%, and 63.74% improvement of RMS values as in the case of the vehicle's lateral, roll, and yaw motions, respectively.

3 Under random track disturbances, the success of the proposed controller has been tested in the frequency domain, and the results are critically analysed in terms of PSDs. It is evident from the results that the FOPID controller using metaheuristic algorithms provides better suppression results of resonant peaks at the extensive range of frequency. The percentage reductions in RMS values for the lateral, roll, and yaw motion were 57.22%, 77.88%, and 69.58%, respectively, compared to the passive system, which is higher than that of classical as well as other metaheuristic (PSO and GWO) techniques.

As a result of the above discussions, it is evident that the ASS with PSO-GWO adjusted FOPID controller demonstrates its usefulness in achieving good vibration attenuation capabilities for railway vehicles under both periodic and random excitations.

In further studies, the performance of an ASS can be enhanced with the help of a multi-objective cost function. Also, the controller parameters could be finely tuned with advanced metaheuristic optimisation techniques that can help to increase ride pleasure.

References

Afolabi Daniyan, I. and Mpofu, K. (2019) 'Vibration analysis and control in the rail car system using PID controls', *Noise Vib. Control – From Theory to Pract.*, pp.1–17, https://doi.org/10.5772/intechopen.85654

Alamdar Ravari, M. and Yaghoobi, M. (2019) 'Optimum design of fractional order pid controller using chaotic firefly algorithms for a control CSTR system', *Asian J, Control*, Vol. 21, pp.2245–2255, https://doi.org/10.1002/asjc.1836

Al-Tashi, Q., Abdul Kadir, S.J., Rais, H.M., Mirjalili, S. and Alhussian, H. (2019) 'Binary optimization using hybrid grey wolf optimization for feature selection', *IEEE Access*, Vol. 7, pp.39496–39508, https://doi.org/10.1109/ACCESS.2019.2906757

Atray, V.S. and Roschke, P.N. (2004) 'Neuro-fuzzy control of railcar vibrations using semiactive dampers', *Comput. Civ. Infrastruct. Eng.*, Vol. 19, pp.81–92, https://doi.org/10.1111/j.1467-8667.2004.00339.x

Babu, Suri, G. and Chiranjeevi, Tirumalasetty (2016) 'Implementation of fractional order PID controller for an AVR system using GA and ACO optimization techniques', *IFAC-PapersOnLine*, Vol. 49, pp.456–461, https://doi.org/10.1016/j.ifacol.2016.03.09639

Baranowski, J., Bauer, W., Zagorowska, M., Dziwinski, T. and Piatek, P. (2015) 'Time-domain oustaloup approximation', *2015 20th Int. Conf. Methods Model. Autom. Robot. MMAR 2015*, 24-27 August, Miedzyzdroje, Poland, pp.116–120, https://doi.org/10.1109/Mmar.2015.7283857

Barbosa, R.S., Tenreiro Machado, J.A. and Jesus, I.S. (2010) 'Effect of fractional orders in the velocity control of a servo system', *Comput. Math. with Appl.*, Vol. 59, pp.1679–1686, https://doi.org/10.1016/j.camwa.2009.08.009

Bingul, Z. and Karahan, O. (2018) 'Comparison of PID and FOPID controllers tuned by PSO and ABC algorithms for unstable and integrating systems with time delay', *Optim. Control Appl. Methods*, Vol. 39, pp.1431–1450, https://doi.org/10.1002/oca.2419

Cao, J.Y., Liang, J. and Cao, B.G. (2005) 'Optimization of fractional order PID controllers based on genetic algorithms', *2005 Int. Conf. Mach. Learn. Cybern. ICMLC 2005*, pp.5686–5689, 18–21 August, Guangzhou, China, https://doi.org/10.1109/icmlc.2005.1527950

Chang, W. and Der, Chen, C.Y. (2014) 'PID controller design for MIMO processes using improved particle swarm optimization', *Circuits, Syst. Signal Process*, Vol. 33, pp.1473–1490, https://doi.org/10.1007/s00034-013-9710-4

Choi, S.B., Choi, J.H., Nam, M.H., Cheong, C.C. and Lee, H.G. (1998) 'A semi-active suspension using ER fluids for a commercial vehicle seat', *J. Intell. Mater. Syst. Struct.*, Vol. 9, pp.601–606, https://doi.org/10.1177/1045389X9800900803

Choi, S.B., Choi, Y.T. and Park, D.W. (2000) 'A sliding mode control of a full-car electrorheological suspension system via hardware in-the-loop simulation', *J. Dyn. Syst. Meas. Control. Trans. ASME*, Vol. 122, pp.114–121, https://doi.org/10.1115/1.482435

Daniyan, I.A., Mpofu, K., Daniyan, O.L. and Adeodu, A.O. (2019) 'Dynamic modelling and simulation of rail car suspension systems using classic controls', *Cogent Eng.*, Vol. 6, pp.1–20, https://doi.org/10.1080/23311916.2019.1602927

Daniyan, I.A., Mpofu, K. and Osadare, D.F. (2018) 'Design and simulation of a controller for an active suspension system of a rail car', *Cogent Eng.*, Vol. 5, pp.1–15, https://doi.org/10.1080/23311916.2018.1545409

Das, S., Saha, S. and Das, Shantanu, Gupta, A. (2011) 'On the selection of tuning methodology of FOPID controllers for the control of higher order processes', *ISA Trans.*, Vol. 50, pp.376–388, https://doi.org/10.1016/j.isatra.2011.02.003

Dastranj, M.R., Rouhani, M. and Hajipoor, A. (2012) 'Design of optimal fractional order PID controller using PSO algorithm', *Int. J. Comput. Theory Eng.*, Vol. 4, pp.429–432, https://doi.org/10.7763/ijcte.2012.v4.499

Debnath, M.K. (2016) 'Technique for automatic generation control of a multi-source power system', *IEEE Uttar Pradesh Sect. Int. Conf. Electr. Comput. Electron. Eng*, 9–11 December, Varanasi, India, pp.531–536.

Dumitriu, M. and Gheti, M.A. (2016) 'Evaluation of the ride quality and ride comfort in railway vehicles based on the index wz', *Int. J. Eng.*, Vol. 13, pp.123–132.

ElMadany, M.M. and Samaha, M.E. (1992) 'On the optimum ride control of a stochastic model of a tractor-semitrailer vehicle', *J. Sound Vib.*, Vol. 156, pp.269–281, https://doi.org/10.1016/0022-460X(92)90697-V

Emary, E., Zawbaa, H.M. and Hassanien, A.E. (2016) 'Binary grey wolf optimization approaches for feature selection', *Neurocomputing*, Vol. 172, pp.371–381, https://doi.org/10.1016/j.neucom.2015.06.083

Eshtay, M., Faris, H. and Obeid, N. (2018) 'Improving extreme learning machine by competitive swarm optimization and its application for medical diagnosis problems', *Expert Syst. Appl.*, Vol. 104, pp.134–152, https://doi.org/10.1016/j.eswa.2018.03.024

Eski, I. and Yildirim, Ş. (2009) 'Vibration control of vehicle active suspension system using a new robust neural network control system. simul', *Model. Pract. Theory*, Vol. 17, pp.778–793, https://doi.org/10.1016/j.simpat.2009.01.004

Fu, B., Giossi, R.L., Persson, R., Stichel, S., Bruni, S. and Goodall, R. (2020) 'Active suspension in railway vehicles: a literature survey', *Railw. Eng. Sci.*, Vol. 28, pp.3–35, https://doi.org/10.1007/s40534-020-00207-w

Gad, S., Metered, H., Bassuiny, A. and Abdel Ghany, A.M. (2015) 'Ride comfort enhancement of heavy vehicles using magnetorheological seat suspension', *Int. J. Heavy Veh. Syst.*, Vol. 22, pp.93–113, https://doi.org/10.1504/IJHVS.2015.070448

Gad, S., Metered, H., Bassuiny, A. and Abdel Ghany, A.M. (2017) 'Multi-objective genetic algorithm fractional-order PID controller for semi-active magnetorheologically damped seat suspension', *JVC/Journal Vib. Control*, Vol. 23, pp.1248–1266, https://doi.org/10.1177/1077546315591620

Ganguly, S., Sahoo, N.C. and Das, D. (2010) 'A novel multi-objective PSO for electrical distribution system planning incorporating distributed generation', *Energy Syst.*, Vol. 1, pp.291–337, https://doi.org/10.1007/s12667-010-0014-5

Goodwin, M.J. (1987) 'Dynamics of railway vehicle systems', *J. Mech. Work. Technol.*, Vol. 14, pp.245–247, https://doi.org/10.1016/0378-3804(87)90070-2

Graa, M., Nejlaoui, M., Houidi, A., Affi, Z. and Romdhane, L. (2018) 'Modeling and control of rail vehicle suspensions: a comparative study based on the passenger comfort', *Proc. Inst. Mech. Eng. Part C, J. Mech. Eng. Sci.*, Vol. 232, pp.260–274, https://doi.org/10.1177/0954406216682542

Hajihassani, M., Jahed Armaghani, D. and Kalatehjari, R. (2018) 'Applications of particle swarm optimization in geotechnical engineering: a comprehensive review', *Geotech. Geol. Eng.*, Vol. 36, pp.705–722, https://doi.org/10.1007/s10706-017-0356-z

He, J., Liu, Z. and Zhang, C. (2020) 'Sliding mode control of lateral semi-active suspension of high-speed train', *J. Adv. Comput. Intell. Intell. Informatics*, Vol. 24, pp.925–933, https://doi.org/10.20965/JACIII.2020.P.0925

Hrovat, D. (1990) 'Optimal active suspension structures for quarter-car vehicle models', *Automatica*, Vol. 26, pp.845–860, https://doi.org/10.1016/0005-1098(90)90002-Y

Hrovat, D. (1993) 'Applications of optimal control to advanced automotive suspension design', *J. Dyn. Syst. Meas. Control. Trans. ASME*, Vol. 115, pp.328–342, https://doi.org/10.1115/1.2899073

Indian Railway Technical Bulletin (2013) Volume LXX, November 2013, Vol. 2557, 4:88-100.

Jain, S. and Hote, Y.V. (2020) 'Design of FOPID controller using BBBC via ZN tuning approach: simulation and experimental validation', *IETE J, Res.*, Vol. 68, pp.1–15, https://doi.org/10.1080/03772063.2020.1756937

Joseph, S.B., Dada, E.G., Abidemi, A., Oyewola, D.O. and Khammas, B.M. (2022) *Metaheuristic Algorithms for PID Controller Parameters Tuning: Review, Approaches and Open Problems*. Heliyon, https:// doi:org/10.1016/j.heliyon.2022.e09399

Kalaivani, R., Lakshmi, P. and Sudhagar, K. (2014) 'Vibration control of vehicle active suspension system using novel fuzzy logic controller', *Int. J. Enterp. Netw. Manag.*, Vol. 6, pp.139–152, https://doi.org/10.1504/IJENM.2014.066824

Karkoub, M.A. and Zribi, M. (2006) 'Active/semi-active suspension control using magnetorheological actuators', *Int. J. Syst. Sci.*, Vol. 37, pp.35–44, https://doi.org/10.1080/00207720500436344

Kim, D.H. and Park, J. (2005) 'Intelligent PID controller tuning of AVR system using GA and PSO', *Lect. Notes Comput. Sci.*, Vol. 3645, pp.366–375, https://doi.org/10.1007/11538356_38

Lanusse, P., Sabatier, J. and Oustaloup, A. (2015) 'Fractional order pid and first generation crone control system design', *Intelligent Systems, Control and Automation: Science and Engineering*, Springer, pp.63–105.

Lei, Y. and Wu, D.T. (2011) 'A new decentralized control approach for the benchmark problem', *Procedia Eng.*, Vol. 14, pp.1229–1236, https://doi.org/10.1016/j.proeng.2011.07.154

Lengare, M.J., Chile, R.H. and Waghmare, L.M. (2012) 'Design of decentralized controllers for MIMO processes', *Comput. Electr. Eng.*, Vol. 38, pp.140–147, https://doi.org/10.1016/j.compeleceng.2011.11.027

Lewis, R. and Olofsson, U. (2006) 'Chapter 5: tribology of the wheel–rail contact', *Handb. Railw. Veh. Dyn.*, p.131.

Li, L., Sun, L., Guo, J., Qi, J., Xu, B. and Li, S. (2017) 'Modified discrete grey wolf optimizer algorithm for multilevel image thresholding', *Comput. Intell. Neurosci.*, Vol. 2017, Article ID 3295769, https://doi.org/10.1155/2017/3295769

Li, T., He, Y., Wang, N., Feng, J., Gui, W. and Zhao, K. (2021) 'Active noise cancellation of rail vehicles based on a convolutional fuzzy neural network prediction approach', *2021 IEEE Veh. Power Propuls. Conf. VPPC 2021 -Proc.*, pp.1–5, https://doi.org/10.1109/VPPC53923.2021.9699325

Luo, Y., Liu, H., Jia, L. and Cai, W. (2011) 'A practical guideline to control structure selection for MIMO processes', *IEEE Int. Conf. Autom. Logist. ICAL*, 15-16 August, Chongqing, China, pp.405–410, https://doi.org/10.1109/ICAL.2011.6024752

Metin, M. and Guclu, R. (2011) 'Active vibration control with comparative algorithms of half rail vehicle model under various track irregularities', *JVC/Journal Vib. Control*, Vol. 17, pp.1525–1539, https://doi.org/10.1177/1077546310381099

Metin, M. and Guclu, R. (2014) 'Rail vehicle vibrations control using parameters adaptive PID controller', *Math. Probl. Eng.*, Vol. 2014, Article ID 728946, https://doi.org/10.1155/2014/728946

Miller, L. (1988) 'tuning passive, semi-active, and fully active suspension systems', *Proceedings of the 27th IEEE Conference on Decision and Control*, 7–9 December, Texas, USA, pp.2047–2053, https://doi.org//10.1109/1988/194694

Mirjalili, S., Mirjalili, S.M. and Lewis, A. (2014) 'Grey wolf optimizer', *Adv. Eng. Softw.*, Vol. 69, pp.46–61, https://doi.org/10.1016/j.advengsoft.2013.12.007

Molatefi, H., Ayoubi, P. and Mozafari, H. (2017) 'Active vibration control of a railway vehicle carbody using piezoelectric elements', *Chinese J, Mech. Eng (English Ed.)*, Vol. 30, pp.963–972, https://doi.org/10.1007/s10033-017-0157-6

Nguyen, S.D. and Nguyen, Q.H. (2017) 'Design of active suspension controller for train cars based on sliding mode control, uncertainty observer and neuro-fuzzy system', *JVC/Journal Vib. Control*, Vol. 23, pp.1334–1353, https://doi.org/10.1177/1077546315592767

Oesterling, B., You, H., Lowe, B.D., Gilmore, B.J. and Freivalds, A. (1999) 'Vibration isolation evaluation of transit bus operator seats based on lower torso acceleration', *Heavy Veh. Syst.*, Vol. 6, pp.374–390, https://doi.org/10.1504/ijhvs.1999.054642

Olivier, M. and Sohn, J.W. (2021) 'Design optimization and performance evaluation of hybrid type magnetorheological damper', *J. Mech. Sci. Technol.*, Vol. 35, pp.3549–3558, https://doi.org/10.1007/s12206-021-0726-6

Orukpe, P.E. (2013) 'Model predictive control application to flexible-bodied railway vehicles for vibration suppression', *Int. J. Eng. Res. Africa*, Vol. 10, pp.25–35, https://doi.org/10.4028/www.scientific.net/JERA.10.25

Orukpe, P.E., Zheng, X., Jaimoukha, I.M., Zolotas, A.C. and Goodall, R.M. (2008) 'Model predictive control based on mixed H2/H∞ control approach for active vibration control of railway vehicles', *Veh. Syst. Dyn.*, Vol. 46, pp.151–160, https://doi.org/10.1080/00423110701882371

Peng, C. and Lines, J.A. (1997) 'Ground induced vibration on unsuspended agricultural tractors', *Heavy Veh. Syst.*, Vol. 4, pp.166–182.

Rabinow, J. (1948) 'The magnetic fluid clutch', *Trans. Am. Inst. Electr. Eng.*, Vol. 67, pp.1308–1315, https://doi.org/10.1109/T-Aiee.1948.5059821

Rajakumar, R., Amudhavel, J., Dhavachelvan, P. and Vengattaraman, T. (2017) 'GWO-lPWSN: grey wolf optimization algorithm for node localization problem in wireless sensor networks', *J. Comput. Networks Commun.*, https://doi.org/10.1155/2017/7348141

Ranganathan, R. and Mohan, M.V. (1997) 'A review of the general effects of whole-body vibration', *Heavy Veh. Syst.*, Vol. 4, pp.353–372.

Reina, G. and Delle Rose, G. (2016) 'Active vibration absorber for automotive suspensions: a theoretical study', *Int. J. Heavy Veh. Syst.*, Vol. 23, pp.21–39, https://doi.org/10.1504/IJHVS.2016.074625

Ren, J., Chen, Z., Yang, Y., Sun, M., Sun, Q. and Wang, Z. (2022) 'Grey wolf optimization based active disturbance rejection control parameter tuning for ship course', *Int. J. Control. Autom. Syst.*, Vol. 20, pp.842–856, https://doi.org/10.1007/s12555-021-0062-8

Sezer, S. and Atalay, A.E. (2011) 'Dynamic modeling and fuzzy logic control of vibrations of a railway vehicle for different track irregularities', *Simul. Model. Pract. Theory*, Vol. 19, pp.1873–1894, https://doi.org/10.1016/j.simpat.2011.04.009

Sharma, P., Gupta, A., Aggarwal, A., Gupta, D., Khanna, A., Hassanien, A.E. and de Albuquerque, V.H.C. (2020) 'The health of things for classification of protein structure using improved grey wolf optimization', *J. Supercomput*., Vol. 76, pp.1226–1241, https://doi.org/10.1007/s11227-018-2639-4

Sharma, P., Sundaram, S., Sharma, M., Sharma, A. and Gupta, D. (2019) 'Diagnosis of parkinson's disease using modified grey wolf optimization. *Cogn. Syst. Res*., Vol. 54, pp.100–115, https://doi.org/10.1016/j.cogsys.2018.12.002

Shie, F.S., Chen, M.Y. and Liu, Y.S. (2012) 'Prediction of corporate financial distress: an application of the america banking industry', *Neural Comput. Appl.*, Vol. 21, pp.1687–1696, https://doi.org/10.1007/s00521-011-0765-5

Sims, N.D. and Stanway, R. (2003) 'Semi-active vehicle suspension using smart fluid dampers: a modelling and control study', *Int. J. Veh. Des.*, Vol. 33, pp.76–102, https://doi.org/10.1504/ijvd.2003.003568

Singh, S.D., Mathur, R. and Srivastava, R.K. (2017) 'Dynamic response of linke hofmann busch (LHB) rail coach considering suspended equipments', *Indian J, Sci. Technol*., Vol. 10, pp.1–20, https://doi.org/10.17485/ijst/2017/v10i38/112223

Slowik, A. (2011) *Particle Swarm Optimization*, Ind. Electron. Handb. – Five Vol. Set 1942–1948, https://doi.org/10.1007/978-3-319-46173-1_2

Sule, A.H., Mokhtar, A.S., Jamian, J.J., Khidrani, B.A. and Larik, R.M. (2020) 'Optimal tuning of proportional integral controller for fixed-speed wind turbine using grey wolf optimizer', *Int. J. Electr. Comput. Eng.*, Vol. 10, pp.5251–5261, https://doi.org/10.11591/IJECE.V10I5.pp.5251–5261

Valério, D. and da Costa, J.S. (2006) 'Tuning of fractional PID controllers with Ziegler-Nichols-type rules', *Signal Processing*, Vol. 86, pp.2771–2784, https://doi.org/10.1016/j.sigpro.2006.02.020

Verma, S.K., Yadav, S. and Nagar, S.K. (2017) 'Optimization of fractional order PID controller using grey wolf optimizer', *J. Control. Autom. Electr. Syst.*, Vol. 28, pp.314–322, https://doi.org/10.1007/s40313-017-0305-3

Wang, D.H. and Liao, W.H. (2009a) 'Semi-active suspension systems for railway vehicles using magnetorheological dampers. part I: system integration and modelling', *Veh. Syst. Dyn.*, Vol. 47, pp.1305–1325, https://doi.org/10.1080/00423110802538328

Wang, D.H. and Liao, W.H. (2009b) 'Semi-active suspension systems for railway vehicles using magnetorheological dampers. part II: simulation and analysis', *Veh. Syst. Dyn.*, Vol. 47, pp.1439–1471, https://doi.org/10.1080/00423110802538336

Wang, H. (2020) 'Active fault tolerance control for active suspension with control input time-delay and actuator gain variation fault', *Int. J. Heavy Veh. Syst.*, Vol. 27, pp.703–722, https://doi.org/10.1504/ijhvs.2020.111260

Wang, K., Shi, Z. and Wang, S. (2019) 'Irregularity model of welded rail joint and wheel-rail dynamic responses in heavy-haul railway', *Int. J. Heavy Veh. Syst.*, Vol. 26, pp.727–745, https://doi.org/10.1504/IJHVS.2019.101893

Wang, P., Li, H., Zhang, J. and Mei, T. (2015) 'An analytical design approach for self-powered active lateral secondary suspensions for railway vehicles', *Veh. Syst. Dyn.*, Vol. 53, pp.1439–1454, https://doi.org/10.1080/00423114.2015.1050964

Wei, X., Zhu, M. and Jia, L. (2016) 'A semi-active control suspension system for railway vehicles with magnetorheological fluid dampers', *Veh. Syst. Dyn.*, Vol. 54, pp.982–1003, https://doi.org/10.1080/00423114.2016.1177189

Winslow, W. (1947) *Method and Means for Translating Electrical Impulses Into Mechanical Force*, US Pat. 2,417,850 6.

Wu, X. and Griffin, M.J. (1997) 'A semi-active control policy to reduce the occurrence and severity of end-stop impacts in a suspension seat with an electrorheological fluid damper', *J. Sound Vib.*, Vol. 203, pp.781–793, https://doi.org/10.1006/jsvi.1996.0901

Yoshimura, T., Edokoro, K. and Ananthanarayana, N. (1993) 'An active suspension model for rail/vehicle systems with preview and stochastic optimal control', *J. Sound Vib.*, Vol. 166, pp.507–519, https://doi.org/10.1006/jsvi.1993.1309

Zhai, W. (2020) *Vehicle – Track Coupled Dynamics*, https://doi.org/10.1007/978-981-32-9283-3

Zong, L.H., Gong, X.L., Xuan, S.H. and Guo, C.Y. (2013) 'Semi-active H∞ control of high-speed railway vehicle suspension with magnetorheological dampers', *Veh. Syst. Dyn.*, Vol. 51, pp.600–626, https://doi.org/10.1080/00423114.2012.758858

Abbreviations

ABC	Artificial bee colony
ACO	Ant colony optimisation
ASS	Active suspension system
AVRS	Automatic voltage regulator system
CC	Cohen coon
CSTR	Continues stirred tank reactor
DOF	Degree of freedom
ER	Electro rheological
FOMCON	Fractional order modelling and control
FOPID	Fractional order proportional integral derivative
GA	Genetic algorithm
GWO	Grey wolf optimisation
MIMO	Multi input multi output
MR	Magneto rheological
MSE	Mean square error
MTSE	Mean time square error
PID	Proportional integral derivative
PSD	Power spectral density
PSO	Particle swarm optimisation
RDSO	Research design and standard organisation
RMS	Root mean square
Z-N	Ziegler-Nichols

Appendix 1: Various parameters used in modelling and simulations

Symbols	*Values*	*Units*	*Definitions*
M_c	41,600	kg	Mass of Car body
J_{cx}	8.95×10^4	$kg.m^2$	Roll moment of inertial of car body
J_{cy}	2.48×10^6	$kg.m^2$	Pitch moment of inertial of car body
J_{cz}	2.52×10^6	$kg.m^2$	Yaw moment of inertia of car body
M_t	3200	kg	Mass of bogie
J_{tx}	3000	$kg.m^2$	Roll moment of inertia
J_{ty}	3000	$kg.m^2$	Pitch moment of inertia
J_{tz}	4280	$kg.m^2$	Yaw moment of inertial of bogie
M_w	1600	kg	Mass of wheelset
J_{tz}	4000	$kg.m^2$	Yaw moment of inertial of wheelset
W	1.25×10^5	N	Load per wheelset
K_{2x}	1.6×10^5	N/m	Secondary longitudinal stiffness
K_{2y}	1.25×10^5	N/m	Secondary lateral stiffness
K_{2z}	3.08×10^5	N/m	Secondary vertical stiffness
K_{1x}	4.2×10^5	N/m	Primary longitudinal stiffness
K_{1y}	0.75×10^7	N/m	Primary lateral stiffness
K_{1z}	1.10×10^6	N/m	Primary vertical stiffness
K_{Gz}	1.25×10^5	N/m	Vertical gravitational stiffness
K_{Gy}	7.5×10^3	N/m	Lateral gravitational stiffness
C_{2y}	–	N.s/m	Secondary lateral damping
C_{2z}	–	N.s/m	Secondary vertical damping
C_{1y}	–	N.s/m	Primary lateral damping
C_{1z}	–	N.s/m	Primary vertical damping
h_3	0.78	m	Vertical distance from car body centre of gravity to lateral secondary suspension
h_2	0.22	m	Vertical distance from bogie centre of gravity to lateral secondary suspension
h_1	–0.2085	m	Vertical distance from bogie centre of gravity to lateral primary suspension
l_b	9	m	Distance from car body centre of gravity to vertical secondary stiffness
l_d	1.28	m	Distance from bogie centre of gravity to vertical primary stiffness
λ_e	0.05		Effective wheel conicity

σ	0.05		Wheelset roll coefficient
a	0.8751	m	wheelbase contact distance
b_1	1	m	Vertical primary suspension spacing
b_2	1	m	Vertical secondary suspension spacing
d_p	1	m	Lateral primary suspension spacing
d_s	1	m	Lateral secondary suspension spacing
R_1	0.4575	m	Vertical distance of lateral primary stiffness to track
f_{11}	1.12×10^7		Longitudinal creep coefficient
f_{22}	9.98×10^6		Lateral creep coefficient

Appendix 2: Pseudo-code of PSO and GWO

PSO

Define objective function

$J(x_1, x_2) = \int r_1.x_1 + r_2.x_2$ //using equation (33)

Set known parameters of railway vehicle// Appendix 1

Parameter setting

Lower Bound & Upper Bound

$[K_P, K_I, K_D]$ =[10 - 10^5]

$[\lambda, \mu] = [0 \ -2]$

Population size (N = 100)

Inertial weight, w, ($w_{max} = 0.9$ *and*, $w_{min} = 0.4$)

Acceleration factors (c_1 *and*, $c_2 = 2$)

Maximum iteration (T = 100)

Initialisation

Generate N particles with random velocities(v_i) and particles (z_i)

Calculate the fitness of each particle in the swarm

Set iteration = 0

Update the *pBest* and *gBest* values

Update the position and velocity of each particle

Set iteration = 1

while t < T

$$w = w_{max} - [(w_{max} - w_{min}) \frac{iteration}{T}]$$

for i = 1:N

GWO

Define objective function

$J(x_1, x_2) = \int r_1.x_1 + r_2.x_2$

//using equation (33)

Set known parameters of railway vehicle// Appendix 1

Parameter setting

Lower Bound & Upper Bound

$[K_P, K_I, K_D]$ =[10 - 10^5]

$[\lambda, \mu] = [0 \ -2]$

Population size (N = 100)

Maximum iteration (T = 100)

Initialisation

Randomly initialise Grey wolf population P

Initialise a, A and C

a linearly decreasing from 2 to 0

$A = 2ar_1 - a$, $C = 2r_2$ // r_1 and r_2 are random vectors [0, 1]

Calculate the fitness of each search agent

$X_{\alpha} =$ Best search agent

$X_{\beta} =$ Second Best search agent

$X_{\delta} =$ Third Best search agent

while $t < T$

for i = 1:N

Update the distance and position of each search agent

Calculate the fitness value $f_{i,j}^{k}$	$Dist = \left\| C.X_p(t) - X(t) \right\|, X_i = X_p(t) - ADist,$
Update the velocity and position	$p = \alpha, \beta, \delta \; and \; i = 1,2,3$
$v_{i,j}^{k+1} = w.v_{i,j}^{k} + c_1 r_1 \left(pBest_{i,j}^{k} - z_{i,j}^{k} \right) + c_1 r_1 \left(gBest_{i,j}^{k} - z_{i,j}^{k} \right)$	$X(t+1) = \frac{X_1 + X_2 + X_3}{3}$
$z_{i,j}^{k+1} = z_{i,j}^{k} + v_{i,j}^{k}$	***end for***
Calculate the fitness $F_i^{k+1} = J\ (z_i^{k+1})$, find the index of best particle	Update a, A and C
end for	Calculate the fitness value f
If the fitness increases then update the *pBest* and *gBest* value	Update X_α, X_β, and X_δ
end while	$t = t + 1$
Display the optimum solution *Guest*	***end while***
	Display the optimum solution